

Partial wave analysis of $J/\psi \rightarrow \gamma\gamma\phi$

The BESIII Collaboration



M. Ablikim¹, M. N. Achasov^{5,b}, P. Adlarson⁷⁴, X. C. Ai⁸⁰, R. Aliberti³⁵,
 A. Amoroso^{73A,73C}, M. R. An³⁹, Q. An^{70,57}, Y. Bai⁵⁶, O. Bakina³⁶, I. Balossino^{29A},
 Y. Ban^{46,g}, V. Batozskaya^{1,44}, K. Begzsuren³², N. Berger³⁵, M. Berlowski⁴⁴,
 M. Bertani^{28A}, D. Bettoni^{29A}, F. Bianchi^{73A,73C}, E. Bianco^{73A,73C}, A. Bortone^{73A,73C},
 I. Boyko³⁶, R. A. Briere⁶, A. Brueggemann⁶⁷, H. Cai⁷⁵, X. Cai^{1,57}, A. Calcaterra^{28A},
 G. F. Cao^{1,62}, N. Cao^{1,62}, S. A. Cetin^{61A}, J. F. Chang^{1,57}, T. T. Chang⁷⁶,
 W. L. Chang^{1,62}, G. R. Che⁴³, G. Chelkov^{36,a}, C. Chen⁴³, Chao Chen⁵⁴, G. Chen¹,
 H. S. Chen^{1,62}, M. L. Chen^{1,57,62}, S. J. Chen⁴², S. M. Chen⁶⁰, T. Chen^{1,62},
 X. R. Chen^{31,62}, X. T. Chen^{1,62}, Y. B. Chen^{1,57}, Y. Q. Chen³⁴, Z. J. Chen^{25,h},
 W. S. Cheng^{73C}, S. K. Choi^{11A}, X. Chu⁴³, G. Cibinetto^{29A}, S. C. Coen⁴, F. Cossio^{73C},
 J. J. Cui⁴⁹, H. L. Dai^{1,57}, J. P. Dai⁷⁸, A. Dbeyssi¹⁸, R. E. de Boer⁴, D. Dedovich³⁶,
 Z. Y. Deng¹, A. Denig³⁵, I. Denysenko³⁶, M. Destefanis^{73A,73C}, F. De Mori^{73A,73C},
 B. Ding^{65,1}, X. X. Ding^{46,g}, Y. Ding⁴⁰, Y. Ding³⁴, J. Dong^{1,57}, L. Y. Dong^{1,62},
 M. Y. Dong^{1,57,62}, X. Dong⁷⁵, M. C. Du¹, S. X. Du⁸⁰, Z. H. Duan⁴², P. Egorov^{36,a},
 Y. H. Y. Fan⁴⁵, Y. L. Fan⁷⁵, J. Fang^{1,57}, S. S. Fang^{1,62}, W. X. Fang¹, Y. Fang¹,
 R. Farinelli^{29A}, L. Fava^{73B,73C}, F. Feldbauer⁴, G. Felici^{28A}, C. Q. Feng^{70,57},
 J. H. Feng⁵⁸, K. Fischer⁶⁸, M. Fritsch⁴, C. Fritsch⁶⁷, C. D. Fu¹, J. L. Fu⁶²,
 Y. W. Fu¹, H. Gao⁶², Y. N. Gao^{46,g}, Yang Gao^{70,57}, S. Garbolino^{73C}, I. Garzia^{29A,29B},
 P. T. Ge⁷⁵, Z. W. Ge⁴², C. Geng⁵⁸, E. M. Gersabeck⁶⁶, A. Gilman⁶⁸, K. Goetzen¹⁴,
 L. Gong⁴⁰, W. X. Gong^{1,57}, W. Gradl³⁵, S. Gramigna^{29A,29B}, M. Greco^{73A,73C},
 M. H. Gu^{1,57}, C. Y. Guan^{1,62}, Z. L. Guan²², A. Q. Guo^{31,62}, L. B. Guo⁴¹, M. J. Guo⁴⁹,
 R. P. Guo⁴⁸, Y. P. Guo^{13,f}, A. Guskov^{36,a}, T. T. Han¹, W. Y. Han³⁹, X. Q. Hao¹⁹,
 F. A. Harris⁶⁴, K. K. He⁵⁴, K. L. He^{1,62}, F. H. Heinsius⁴, C. H. Heinz³⁵,
 Y. K. Heng^{1,57,62}, C. Herold⁵⁹, T. Holtmann⁴, P. C. Hong^{13,f}, G. Y. Hou^{1,62},
 X. T. Hou^{1,62}, Y. R. Hou⁶², Z. L. Hou¹, H. M. Hu^{1,62}, J. F. Hu^{55,i}, T. Hu^{1,57,62},
 Y. Hu¹, G. S. Huang^{70,57}, K. X. Huang⁵⁸, L. Q. Huang^{31,62}, X. T. Huang⁴⁹,
 Y. P. Huang¹, T. Hussain⁷², N. Hüsken^{27,35}, W. Imoehl²⁷, J. Jackson²⁷, S. Jaeger⁴,
 S. Janchiv³², J. H. Jeong^{11A}, Q. Ji¹, Q. P. Ji¹⁹, X. B. Ji^{1,62}, X. L. Ji^{1,57}, Y. Y. Ji⁴⁹,
 X. Q. Jia⁴⁹, Z. K. Jia^{70,57}, H. J. Jiang⁷⁵, P. C. Jiang^{46,g}, S. S. Jiang³⁹, T. J. Jiang¹⁶,
 X. S. Jiang^{1,57,62}, Y. Jiang⁶², J. B. Jiao⁴⁹, Z. Jiao²³, S. Jin⁴², Y. Jin⁶⁵, M. Q. Jing^{1,62},
 T. Johansson⁷⁴, X. K.¹, S. Kabana³³, N. Kalantar-Nayestanaki⁶³, X. L. Kang¹⁰,

X. S. Kang⁴⁰, M. Kavatsyuk⁶³, B. C. Ke⁸⁰, A. Khoukaz⁶⁷, R. Kiuchi¹, R. Kliemt¹⁴, O. B. Kolcu^{61A}, B. Kopf⁴, M. Kuessner⁴, A. Kupsc^{44,74}, W. Kühn³⁷, J. J. Lane⁶⁶, P. Larin¹⁸, A. Lavania²⁶, L. Lavezzi^{73A,73C}, T. T. Lei^{70,57}, Z. H. Lei^{70,57}, H. Leithoff³⁵, M. Lellmann³⁵, T. Lenz³⁵, C. Li⁴³, C. Li⁴⁷, C. H. Li³⁹, Cheng Li^{70,57}, D. M. Li⁸⁰, F. Li^{1,57}, G. Li¹, H. Li^{70,57}, H. B. Li^{1,62}, H. J. Li¹⁹, H. N. Li^{55,i}, Hui Li⁴³, J. R. Li⁶⁰, J. S. Li⁵⁸, J. W. Li⁴⁹, K. L. Li¹⁹, Ke Li¹, L. J. Li^{1,62}, L. K. Li¹, Lei Li³, M. H. Li⁴³, P. R. Li^{38,j,k}, Q. X. Li⁴⁹, S. X. Li¹³, T. Li⁴⁹, W. D. Li^{1,62}, W. G. Li¹, X. H. Li^{70,57}, X. L. Li⁴⁹, Xiaoyu Li^{1,62}, Y. G. Li^{46,g}, Z. J. Li⁵⁸, C. Liang⁴², H. Liang³⁴, H. Liang^{1,62}, H. Liang^{70,57}, Y. F. Liang⁵³, Y. T. Liang^{31,62}, G. R. Liao¹⁵, L. Z. Liao⁴⁹, Y. P. Liao^{1,62}, J. Libby²⁶, A. Limphirat⁵⁹, D. X. Lin^{31,62}, T. Lin¹, B. J. Liu¹, B. X. Liu⁷⁵, C. Liu³⁴, C. X. Liu¹, F. H. Liu⁵², Fang Liu¹, Feng Liu⁷, G. M. Liu^{55,i}, H. Liu^{38,j,k}, H. M. Liu^{1,62}, Huanhuan Liu¹, Huihui Liu²¹, J. B. Liu^{70,57}, J. L. Liu⁷¹, J. Y. Liu^{1,62}, K. Liu¹, K. Y. Liu⁴⁰, Ke Liu²², L. Liu^{70,57}, L. C. Liu⁴³, Lu Liu⁴³, M. H. Liu^{13,f}, P. L. Liu¹, Q. Liu⁶², S. B. Liu^{70,57}, T. Liu^{13,f}, W. K. Liu⁴³, W. M. Liu^{70,57}, X. Liu^{38,j,k}, Y. Liu^{38,j,k}, Y. Liu⁸⁰, Y. B. Liu⁴³, Z. A. Liu^{1,57,62}, Z. Q. Liu⁴⁹, X. C. Lou^{1,57,62}, F. X. Lu⁵⁸, H. J. Lu²³, J. G. Lu^{1,57}, X. L. Lu¹, Y. Lu⁸, Y. P. Lu^{1,57}, Z. H. Lu^{1,62}, C. L. Luo⁴¹, M. X. Luo⁷⁹, T. Luo^{13,f}, X. L. Luo^{1,57}, X. R. Lyu⁶², Y. F. Lyu⁴³, F. C. Ma⁴⁰, H. L. Ma¹, J. L. Ma^{1,62}, L. L. Ma⁴⁹, M. M. Ma^{1,62}, Q. M. Ma¹, R. Q. Ma^{1,62}, R. T. Ma⁶², X. Y. Ma^{1,57}, Y. Ma^{46,g}, Y. M. Ma³¹, F. E. Maas¹⁸, M. Maggiora^{73A,73C}, S. Malde⁶⁸, Q. A. Malik⁷², A. Mangoni^{28B}, Y. J. Mao^{46,g}, Z. P. Mao¹, S. Marcello^{73A,73C}, Z. X. Meng⁶⁵, J. G. Messchendorp^{14,63}, G. Mezzadri^{29A}, H. Miao^{1,62}, T. J. Min⁴², R. E. Mitchell²⁷, X. H. Mo^{1,57,62}, N. Yu. Muchnoi^{5,b}, J. Muskalla³⁵, Y. Nefedov³⁶, F. Nerling^{18,d}, I. B. Nikolaev^{5,b}, Z. Ning^{1,57}, S. Nisar^{12,l}, Y. Niu⁴⁹, S. L. Olsen⁶², Q. Ouyang^{1,57,62}, S. Pacetti^{28B,28C}, X. Pan⁵⁴, Y. Pan⁵⁶, A. Pathak³⁴, P. Patteri^{28A}, Y. P. Pei^{70,57}, M. Pelizaeus⁴, H. P. Peng^{70,57}, K. Peters^{14,d}, J. L. Ping⁴¹, R. G. Ping^{1,62}, S. Plura³⁵, S. Pogodin³⁶, V. Prasad³³, F. Z. Qi¹, H. Qi^{70,57}, H. R. Qi⁶⁰, M. Qi⁴², T. Y. Qi^{13,f}, S. Qian^{1,57}, W. B. Qian⁶², C. F. Qiao⁶², J. J. Qin⁷¹, L. Q. Qin¹⁵, X. P. Qin^{13,f}, X. S. Qin⁴⁹, Z. H. Qin^{1,57}, J. F. Qiu¹, S. Q. Qu⁶⁰, C. F. Redmer³⁵, K. J. Ren³⁹, A. Rivetti^{73C}, M. Rolo^{73C}, G. Rong^{1,62}, Ch. Rosner¹⁸, S. N. Ruan⁴³, N. Salone⁴⁴, A. Sarantsev^{36,c}, Y. Schelhaas³⁵, K. Schoenning⁷⁴, M. Scodiggio^{29A,29B}, K. Y. Shan^{13,f}, W. Shan²⁴, X. Y. Shan^{70,57}, J. F. Shangguan⁵⁴, L. G. Shao^{1,62}, M. Shao^{70,57}, C. P. Shen^{13,f}, H. F. Shen^{1,62}, W. H. Shen⁶², X. Y. Shen^{1,62}, B. A. Shi⁶², H. C. Shi^{70,57}, J. L. Shi¹³, J. Y. Shi¹, Q. Q. Shi⁵⁴, R. S. Shi^{1,62}, X. Shi^{1,57}, J. J. Song¹⁹, T. Z. Song⁵⁸, W. M. Song^{34,1}, Y. J. Song¹³, Y. X. Song^{46,g}, S. Sosio^{73A,73C}, S. Spataro^{73A,73C}, F. Stieler³⁵, Y. J. Su⁶², G. B. Sun⁷⁵, G. X. Sun¹, H. Sun⁶², H. K. Sun¹, J. F. Sun¹⁹, K. Sun⁶⁰, L. Sun⁷⁵, S. S. Sun^{1,62}, T. Sun^{1,62}, W. Y. Sun³⁴, Y. Sun¹⁰, Y. J. Sun^{70,57}, Y. Z. Sun¹, Z. T. Sun⁴⁹, Y. X. Tan^{70,57}, C. J. Tang⁵³, G. Y. Tang¹, J. Tang⁵⁸, Y. A. Tang⁷⁵, L. Y. Tao⁷¹, Q. T. Tao^{25,h}, M. Tat⁶⁸, J. X. Teng^{70,57}, V. Thoren⁷⁴, W. H. Tian⁵¹, W. H. Tian⁵⁸, Y. Tian^{31,62}, Z. F. Tian⁷⁵, I. Uman^{61B}, S. J. Wang⁴⁹, B. Wang¹, B. L. Wang⁶², Bo Wang^{70,57}, C. W. Wang⁴², D. Y. Wang^{46,g}, F. Wang⁷¹, H. J. Wang^{38,j,k}, H. P. Wang^{1,62}, J. P. Wang⁴⁹, K. Wang^{1,57}, L. L. Wang¹, M. Wang⁴⁹, Meng Wang^{1,62}, S. Wang^{13,f}, S. Wang^{38,j,k}, T. Wang^{13,f}, T. J. Wang⁴³,

W. Wang⁵⁸, W. Wang⁷¹, W. P. Wang^{70,57}, X. Wang^{46,g}, X. F. Wang^{38,j,k},
X. J. Wang³⁹, X. L. Wang^{13,f}, Y. Wang⁶⁰, Y. D. Wang⁴⁵, Y. F. Wang^{1,57,62},
Y. H. Wang⁴⁷, Y. N. Wang⁴⁵, Y. Q. Wang¹, Yaqian Wang^{17,1}, Yi Wang⁶⁰,
Z. Wang^{1,57}, Z. L. Wang⁷¹, Z. Y. Wang^{1,62}, Ziyi Wang⁶², D. Wei⁶⁹, D. H. Wei¹⁵,
F. Weidner⁶⁷, S. P. Wen¹, C. W. Wenzel⁴, U. Wiedner⁴, G. Wilkinson⁶⁸, M. Wolke⁷⁴,
L. Wollenberg⁴, C. Wu³⁹, J. F. Wu^{1,62}, L. H. Wu¹, L. J. Wu^{1,62}, X. Wu^{13,f},
X. H. Wu³⁴, Y. Wu⁷⁰, Y. J. Wu³¹, Z. Wu^{1,57}, L. Xia^{70,57}, X. M. Xian³⁹, T. Xiang^{46,g},
D. Xiao^{38,j,k}, G. Y. Xiao⁴², S. Y. Xiao¹, Y. L. Xiao^{13,f}, Z. J. Xiao⁴¹, C. Xie⁴²,
X. H. Xie^{46,g}, Y. Xie⁴⁹, Y. G. Xie^{1,57}, Y. H. Xie⁷, Z. P. Xie^{70,57}, T. Y. Xing^{1,62},
C. F. Xu^{1,62}, C. J. Xu⁵⁸, G. F. Xu¹, H. Y. Xu⁶⁵, Q. J. Xu¹⁶, Q. N. Xu³⁰, W. Xu^{1,62},
W. L. Xu⁶⁵, X. P. Xu⁵⁴, Y. C. Xu⁷⁷, Z. P. Xu⁴², Z. S. Xu⁶², F. Yan^{13,f}, L. Yan^{13,f},
W. B. Yan^{70,57}, W. C. Yan⁸⁰, X. Q. Yan¹, H. J. Yang^{50,e}, H. L. Yang³⁴, H. X. Yang¹,
Tao Yang¹, Y. Yang^{13,f}, Y. F. Yang⁴³, Y. X. Yang^{1,62}, Yifan Yang^{1,62},
Z. W. Yang^{38,j,k}, Z. P. Yao⁴⁹, M. Ye^{1,57}, M. H. Ye⁹, J. H. Yin¹, Z. Y. You⁵⁸,
B. X. Yu^{1,57,62}, C. X. Yu⁴³, G. Yu^{1,62}, J. S. Yu^{25,h}, T. Yu⁷¹, X. D. Yu^{46,g},
C. Z. Yuan^{1,62}, L. Yuan², S. C. Yuan¹, X. Q. Yuan¹, Y. Yuan^{1,62}, Z. Y. Yuan⁵⁸,
C. X. Yue³⁹, A. A. Zafar⁷², F. R. Zeng⁴⁹, X. Zeng^{13,f}, Y. Zeng^{25,h}, Y. J. Zeng^{1,62},
X. Y. Zhai³⁴, Y. C. Zhai⁴⁹, Y. H. Zhan⁵⁸, A. Q. Zhang^{1,62}, B. L. Zhang^{1,62},
B. X. Zhang¹, D. H. Zhang⁴³, G. Y. Zhang¹⁹, H. Zhang⁷⁰, H. H. Zhang⁵⁸,
H. H. Zhang³⁴, H. Q. Zhang^{1,57,62}, H. Y. Zhang^{1,57}, J. Zhang⁸⁰, J. J. Zhang⁵¹,
J. L. Zhang²⁰, J. Q. Zhang⁴¹, J. W. Zhang^{1,57,62}, J. X. Zhang^{38,j,k}, J. Y. Zhang¹,
J. Z. Zhang^{1,62}, Jianyu Zhang⁶², Jiawei Zhang^{1,62}, L. M. Zhang⁶⁰, L. Q. Zhang⁵⁸,
Lei Zhang⁴², P. Zhang^{1,62}, Q. Y. Zhang^{39,80}, Shuihan Zhang^{1,62}, Shulei Zhang^{25,h},
X. D. Zhang⁴⁵, X. M. Zhang¹, X. Y. Zhang⁴⁹, Xuyan Zhang⁵⁴, Y. Zhang⁷¹,
Y. Zhang⁶⁸, Y. T. Zhang⁸⁰, Y. H. Zhang^{1,57}, Yan Zhang^{70,57}, Yao Zhang¹,
Z. H. Zhang¹, Z. L. Zhang³⁴, Z. Y. Zhang⁷⁵, Z. Y. Zhang⁴³, G. Zhao¹, J. Zhao³⁹,
J. Y. Zhao^{1,62}, J. Z. Zhao^{1,57}, Lei Zhao^{70,57}, Ling Zhao¹, M. G. Zhao⁴³, S. J. Zhao⁸⁰,
Y. B. Zhao^{1,57}, Y. X. Zhao^{31,62}, Z. G. Zhao^{70,57}, A. Zhemchugov^{36,a}, B. Zheng⁷¹,
J. P. Zheng^{1,57}, W. J. Zheng^{1,62}, Y. H. Zheng⁶², B. Zhong⁴¹, X. Zhong⁵⁸, H. Zhou⁴⁹,
L. P. Zhou^{1,62}, X. Zhou⁷⁵, X. K. Zhou⁷, X. R. Zhou^{70,57}, X. Y. Zhou³⁹, Y. Z. Zhou^{13,f},
J. Zhu⁴³, K. Zhu¹, K. J. Zhu^{1,57,62}, L. Zhu³⁴, L. X. Zhu⁶², S. H. Zhu⁶⁹, S. Q. Zhu⁴²,
T. J. Zhu^{13,f}, W. J. Zhu^{13,f}, Y. C. Zhu^{70,57}, Z. A. Zhu^{1,62}, J. H. Zou¹, J. Zu^{70,57}

(BESIII Collaboration)

¹ *Institute of High Energy Physics, Beijing 100049, People's Republic of China*

² *Beihang University, Beijing 100191, People's Republic of China*

³ *Beijing Institute of Petrochemical Technology, Beijing 102617, People's Republic of China*

⁴ *Bochum Ruhr-University, D-44780 Bochum, Germany*

⁵ *Budker Institute of Nuclear Physics SB RAS (BINP), Novosibirsk 630090, Russia*

⁶ *Carnegie Mellon University, Pittsburgh, Pennsylvania 15213, USA*

⁷ *Central China Normal University, Wuhan 430079, People's Republic of China*

⁸ *Central South University, Changsha 410083, People's Republic of China*

- ⁹ *China Center of Advanced Science and Technology, Beijing 100190, People's Republic of China*
- ¹⁰ *China University of Geosciences, Wuhan 430074, People's Republic of China*
- ¹¹ *Chung-Ang University, Seoul, 06974, Republic of Korea*
- ¹² *COMSATS University Islamabad, Lahore Campus, Defence Road, Off Raiwind Road, 54000 Lahore, Pakistan*
- ¹³ *Fudan University, Shanghai 200433, People's Republic of China*
- ¹⁴ *GSI Helmholtzcentre for Heavy Ion Research GmbH, D-64291 Darmstadt, Germany*
- ¹⁵ *Guangxi Normal University, Guilin 541004, People's Republic of China*
- ¹⁶ *Hangzhou Normal University, Hangzhou 310036, People's Republic of China*
- ¹⁷ *Hebei University, Baoding 071002, People's Republic of China*
- ¹⁸ *Helmholtz Institute Mainz, Staudinger Weg 18, D-55099 Mainz, Germany*
- ¹⁹ *Henan Normal University, Xinxiang 453007, People's Republic of China*
- ²⁰ *Henan University, Kaifeng 475004, People's Republic of China*
- ²¹ *Henan University of Science and Technology, Luoyang 471003, People's Republic of China*
- ²² *Henan University of Technology, Zhengzhou 450001, People's Republic of China*
- ²³ *Huangshan College, Huangshan 245000, People's Republic of China*
- ²⁴ *Hunan Normal University, Changsha 410081, People's Republic of China*
- ²⁵ *Hunan University, Changsha 410082, People's Republic of China*
- ²⁶ *Indian Institute of Technology Madras, Chennai 600036, India*
- ²⁷ *Indiana University, Bloomington, Indiana 47405, USA*
- ²⁸ *INFN Laboratori Nazionali di Frascati , (A)INFN Laboratori Nazionali di Frascati, I-00044, Frascati, Italy; (B)INFN Sezione di Perugia, I-06100, Perugia, Italy; (C)University of Perugia, I-06100, Perugia, Italy*
- ²⁹ *INFN Sezione di Ferrara, (A)INFN Sezione di Ferrara, I-44122, Ferrara, Italy; (B)University of Ferrara, I-44122, Ferrara, Italy*
- ³⁰ *Inner Mongolia University, Hohhot 010021, People's Republic of China*
- ³¹ *Institute of Modern Physics, Lanzhou 730000, People's Republic of China*
- ³² *Institute of Physics and Technology, Peace Avenue 54B, Ulaanbaatar 13330, Mongolia*
- ³³ *Instituto de Alta Investigación, Universidad de Tarapacá, Casilla 7D, Arica 1000000, Chile*
- ³⁴ *Jilin University, Changchun 130012, People's Republic of China*
- ³⁵ *Johannes Gutenberg University of Mainz, Johann-Joachim-Becher-Weg 45, D-55099 Mainz, Germany*
- ³⁶ *Joint Institute for Nuclear Research, 141980 Dubna, Moscow region, Russia*
- ³⁷ *Justus-Liebig-Universitaet Giessen, II. Physikalisches Institut, Heinrich-Buff-Ring 16, D-35392 Giessen, Germany*
- ³⁸ *Lanzhou University, Lanzhou 730000, People's Republic of China*
- ³⁹ *Liaoning Normal University, Dalian 116029, People's Republic of China*
- ⁴⁰ *Liaoning University, Shenyang 110036, People's Republic of China*
- ⁴¹ *Nanjing Normal University, Nanjing 210023, People's Republic of China*
- ⁴² *Nanjing University, Nanjing 210093, People's Republic of China*

- 43 *Nankai University, Tianjin 300071, People's Republic of China*
- 44 *National Centre for Nuclear Research, Warsaw 02-093, Poland*
- 45 *North China Electric Power University, Beijing 102206, People's Republic of China*
- 46 *Peking University, Beijing 100871, People's Republic of China*
- 47 *Qufu Normal University, Qufu 273165, People's Republic of China*
- 48 *Shandong Normal University, Jinan 250014, People's Republic of China*
- 49 *Shandong University, Jinan 250100, People's Republic of China*
- 50 *Shanghai Jiao Tong University, Shanghai 200240, People's Republic of China*
- 51 *Shanxi Normal University, Linfen 041004, People's Republic of China*
- 52 *Shanxi University, Taiyuan 030006, People's Republic of China*
- 53 *Sichuan University, Chengdu 610064, People's Republic of China*
- 54 *Soochow University, Suzhou 215006, People's Republic of China*
- 55 *South China Normal University, Guangzhou 510006, People's Republic of China*
- 56 *Southeast University, Nanjing 211100, People's Republic of China*
- 57 *State Key Laboratory of Particle Detection and Electronics, Beijing 100049, Hefei 230026, People's Republic of China*
- 58 *Sun Yat-Sen University, Guangzhou 510275, People's Republic of China*
- 59 *Suranaree University of Technology, University Avenue 111, Nakhon Ratchasima 30000, Thailand*
- 60 *Tsinghua University, Beijing 100084, People's Republic of China*
- 61 *Turkish Accelerator Center Particle Factory Group, (A)Istinye University, 34010, Istanbul, Turkey; (B)Near East University, Nicosia, North Cyprus, 99138, Mersin 10, Turkey*
- 62 *University of Chinese Academy of Sciences, Beijing 100049, People's Republic of China*
- 63 *University of Groningen, NL-9747 AA Groningen, The Netherlands*
- 64 *University of Hawaii, Honolulu, Hawaii 96822, USA*
- 65 *University of Jinan, Jinan 250022, People's Republic of China*
- 66 *University of Manchester, Oxford Road, Manchester, M13 9PL, United Kingdom*
- 67 *University of Muenster, Wilhelm-Klemm-Strasse 9, 48149 Muenster, Germany*
- 68 *University of Oxford, Keble Road, Oxford OX13RH, United Kingdom*
- 69 *University of Science and Technology Liaoning, Anshan 114051, People's Republic of China*
- 70 *University of Science and Technology of China, Hefei 230026, People's Republic of China*
- 71 *University of South China, Hengyang 421001, People's Republic of China*
- 72 *University of the Punjab, Lahore-54590, Pakistan*
- 73 *University of Turin and INFN, (A)University of Turin, I-10125, Turin, Italy; (B)University of Eastern Piedmont, I-15121, Alessandria, Italy; (C)INFN, I-10125, Turin, Italy*
- 74 *Uppsala University, Box 516, SE-75120 Uppsala, Sweden*
- 75 *Wuhan University, Wuhan 430072, People's Republic of China*
- 76 *Xinyang Normal University, Xinyang 464000, People's Republic of China*
- 77 *Yantai University, Yantai 264005, People's Republic of China*

⁷⁸ Yunnan University, Kunming 650500, People's Republic of China

⁷⁹ Zhejiang University, Hangzhou 310027, People's Republic of China

⁸⁰ Zhengzhou University, Zhengzhou 450001, People's Republic of China

^a Also at the Moscow Institute of Physics and Technology, Moscow 141700, Russia

^b Also at the Novosibirsk State University, Novosibirsk, 630090, Russia

^c Also at the NRC "Kurchatov Institute", PNPI, 188300, Gatchina, Russia

^d Also at Goethe University Frankfurt, 60323 Frankfurt am Main, Germany

^e Also at Key Laboratory for Particle Physics, Astrophysics and Cosmology, Ministry of Education; Shanghai Key Laboratory for Particle Physics and Cosmology; Institute of Nuclear and Particle Physics, Shanghai 200240, People's Republic of China

^f Also at Key Laboratory of Nuclear Physics and Ion-beam Application (MOE) and Institute of Modern Physics, Fudan University, Shanghai 200443, People's Republic of China

^g Also at State Key Laboratory of Nuclear Physics and Technology, Peking University, Beijing 100871, People's Republic of China

^h Also at School of Physics and Electronics, Hunan University, Changsha 410082, China

ⁱ Also at Guangdong Provincial Key Laboratory of Nuclear Science, Institute of Quantum Matter, South China Normal University, Guangzhou 510006, China

^j Also at Frontiers Science Center for Rare Isotopes, Lanzhou University, Lanzhou 730000, People's Republic of China

^k Also at Lanzhou Center for Theoretical Physics, Lanzhou University, Lanzhou 730000, People's Republic of China

^l Also at the Department of Mathematical Sciences, IBA, Karachi 75270, Pakistan

E-mail: besiii-publications@ihep.ac.cn

ABSTRACT: Using a sample of $(10087 \pm 44) \times 10^6$ J/ψ events collected with the BESIII detector at the BEPCII collider, a partial wave analysis on the decay $J/\psi \rightarrow \gamma\gamma\phi$ is performed to investigate the intermediate resonances in $J/\psi \rightarrow \gamma X, X \rightarrow \gamma\phi$. The resonances $f_1(1285)$, $\eta(1405)$, $f_1(1420)$, $f_1(1510)$, $f_2(1525)$, $X(1835)$, $f_2(1950)$, $f_2(2010)$, $f_0(2200)$ and η_c are observed with statistical significance greater than 5σ . The product branching fractions $\mathcal{B}(J/\psi \rightarrow \gamma X, X \rightarrow \gamma\phi)$ are reported. The resonance parameters of $\eta(1405)$ and $X(1835)$ are also measured.

Contents

1	Introduction	1
2	BESIII Detector and MC Sample	2
3	Event Selection	3
4	Background Treatment	5
4.1	Treatment of non- ϕ background	5
4.2	Treatment of ϕ background	6
5	Partial Wave Analysis	6
6	PWA Results	10
7	Systematic Uncertainties	14
7.1	Systematic uncertainties due to the event selections	14
7.2	Systematic uncertainties due to the PWA	15
8	Summary and Discussion	16
A	Scan Plots For Baseline Solution	21

1 Introduction

The non-abelian nature of quantum chromodynamics (QCD) predicts the existence of various exotic states, including glueballs, hybrids, and multiquark states. The experimental confirmation of these states would yield crucial insight into the confinement regime of QCD and serve as a direct test of QCD theory. Radiative decays of charmonium are glue-rich processes and serve as excellent probes for studying the production of gluonic matter and light hadron structures. While significant progress has been made in the past few decades, numerous unresolved issues persist.

One of the hot topics is the nature of the two pseudoscalar states near $1.4 \text{ GeV}/c^2$, the $\eta(1405)$ and $\eta(1475)$ as listed by the Particle Data Group (PDG) [1]. The $\eta(1475)$ could be interpreted as the first radial excitation of the η' . The $\eta(1405)$ was proposed to be a candidate for the ground state pseudoscalar glueball [2]. However, the mass of $\eta(1405)$ is relatively far from the mass of a pseudoscalar glueball predicted to be $2.3\text{-}2.6 \text{ GeV}/c^2$ by Lattice QCD (LQCD) [3, 4]. This is known as the long standing ‘‘E- ι puzzle’’ [5]. It is still controversial whether the $\eta(1405)$ and $\eta(1475)$ are two separate states or just one pseudoscalar state observed in different decay modes.

The state $\eta(1295)$ is often considered as a possible candidate for the first radial excitation of η . On the other hand, $\eta(1295)$ can also be explained as a misidentified $f_1(1285)$ [6]. A careful study of $\eta(1295)$ is necessary to resolve this problem.

The $X(1835)$ was first observed in the decay $J/\psi \rightarrow \gamma\pi^+\pi^-\eta'$ by BESII [7], and its spin-parity quantum numbers were determined to be $J^{PC} = 0^{-+}$ by BESIII [8]. The discovery of $X(1835)$ stimulated multiple theoretical speculations concerning its nature. Possible interpretations include a $N\bar{N}$ bound state [9], a baryonium with a sizable gluon content [10], a second radial excitation of the η' [11, 12], an η_c -glueball mixture and a pseudoscalar glueball [13]. So far, none of these interpretations has been ruled out or confirmed. In addition, at higher $\pi^+\pi^-\eta'$ invariant masses, the states $X(2120)$, $X(2370)$, $X(2600)$ are also observed by the BESIII collaboration [14, 15]. The measured mass of the $X(2370)$ is consistent with the pseudoscalar glueball candidate predicted by LQCD calculations [16]. To understand the nature of the $X(2370)$, it is critical to measure its quantum numbers and to search for it in more decay modes.

The decays $J/\psi \rightarrow \gamma X$, $X \rightarrow \gamma V$ with $V \equiv \rho, \omega, \phi$, serve as flavor filter reactions and play an important role in unraveling the quark contents of the intermediate resonances [17]. Previously, the BESIII collaboration has studied the prominent features of $f_1(1285)$, $\eta(1475)$, and $X(1835)$ using 1.3 billion J/ψ events [18]. A one-dimensional fit to the $\gamma\phi$ invariant mass ($M(\gamma\phi)$) spectrum from $J/\psi \rightarrow \gamma\gamma\phi$ was performed. In addition, from the angular distribution it was found that the data favor spin and parity (J^{PC}) assignments of 0^{+-} for the structures around 1.4 GeV/ c^2 and 1.8 GeV/ c^2 .

In this paper, we report the results of a partial wave analysis (PWA) of $J/\psi \rightarrow \gamma\gamma\phi$ to extract the contribution of intermediate components. This analysis uses a sample of $(10087 \pm 44) \times 10^6$ J/ψ events collected by the BESIII detector at the BEPCII storage ring [19].

2 BESIII Detector and MC Sample

The BESIII detector [20] records symmetric e^+e^- collisions provided by the BEPCII storage ring [21] in the center-of-mass energy range from 2.0 to 4.95 GeV, with a peak luminosity of 1×10^{33} cm $^{-2}$ s $^{-1}$ achieved at $\sqrt{s} = 3.77$ GeV. BESIII has collected large data samples in this energy region [22][23][24]. The cylindrical core of the BESIII detector covers 93% of the full solid angle and consists of a helium-based multilayer drift chamber (MDC), a plastic scintillator time-of-flight system (TOF), and a CsI(Tl) electromagnetic calorimeter (EMC), which are all enclosed in a superconducting solenoidal magnet providing a 1.0 T magnetic field. The magnetic field was 0.9 T in 2012, which affects 10.8% of the total J/ψ data. The solenoid is supported by an octagonal flux-return yoke with resistive plate counter muon identification modules interleaved with steel. The charged-particle momentum resolution at 1 GeV/ c is 0.5%, and the dE/dx resolution is 6% for electrons from Bhabha scattering. The EMC measures photon energies with a resolution of 2.5% (5%) at 1 GeV in the barrel (end cap) region. The time resolution in the TOF barrel region is 68 ps, while that in the end cap region was 110 ps. The end cap TOF system was upgraded

in 2015 using multigap resistive plate chamber technology, providing a time resolution of 60 ps, which benefits 87.0% of the data used in this analysis [25].

Simulated data samples produced with a GEANT4-based [26] Monte Carlo (MC) package, which includes the geometric description of the BESIII detector and the detector response [27], are used to determine detection efficiencies and to estimate backgrounds. The simulation models the beam energy spread and initial state radiation in the e^+e^- annihilations with the generator KKMC [28]. Signal MC samples for the process $J/\psi \rightarrow \gamma\gamma\phi$ with the subsequent decays $\phi \rightarrow K^+K^-$ are generated uniformly in phase space (PHSP). The inclusive MC sample includes both the production of the J/ψ resonance and the continuum processes which are incorporated in KKMC. All particle decays are modeled with EVTGEN [29] using branching fractions (BF) either taken from the PDG [1], when available, or otherwise estimated with LUNDCHARM [30]. Final state radiation from charged final state particles is incorporated using the PHOTOS package [31].

3 Event Selection

Charged tracks detected in the MDC are required to be within a polar angle (θ) range of $|\cos\theta| < 0.93$, where θ is defined with respect to the z -axis, the symmetry axis of the MDC. The distance of closest approach to the interaction point (IP) must be less than 10 cm along the z -axis and less than 1 cm in the transverse plane. Particle identification (PID) for charged tracks combines measurements of the dE/dx in the MDC and the flight time in the TOF to form likelihoods $\mathcal{L}(h)$ ($h = p, K, \pi$) for each hadron h hypothesis. E.g., a track is identified as a kaon if its kaon hypothesis likelihood satisfies $\mathcal{L}(K) > \mathcal{L}(\pi)$, $\mathcal{L}(K) > \mathcal{L}(p)$. Photon candidates are identified by the showers produced in the EMC. The deposited energy of each shower must be larger than 25 MeV in the barrel region ($|\cos\theta| < 0.80$) and larger than 50 MeV in the end cap regions ($0.86 < |\cos\theta| < 0.92$). To exclude showers that originate from charged tracks, the angle subtended by the EMC shower and the position of the closest charged track at the EMC must be greater than 10 degrees as measured from the IP. To suppress electronic noise and showers unrelated to the event, the difference between the EMC time and the event start time is required to be within $[0, 700]$ ns. Candidate events are required to have two oppositely charged tracks identified as kaons and have at least two photons. A four-constraint (4C) kinematic fit is performed under the $J/\psi \rightarrow \gamma\gamma K^+K^-$ hypothesis, applied to all combinations with good photon candidates. The χ_{4C}^2 of the 4C kinematic fit is required to be less than 40. For events with more than one combination of $J/\psi \rightarrow \gamma\gamma K^+K^-$, only the combination with the minimum χ_{4C}^2 is retained. To suppress possible multi-photon backgrounds, additional 4C kinematic fits for γK^+K^- , $3\gamma K^+K^-$, or $4\gamma K^+K^-$ hypotheses are performed and an event is only retained for further analysis if $\chi_{4C}^2(\gamma\gamma K^+K^-)$ is smaller than χ_{4C}^2 of any of the additional hypotheses. After application of the above selection criteria the distribution of the K^+K^- invariant mass $M(K^+K^-)$ versus the $\gamma\gamma$ invariant mass $M(\gamma\gamma)$ of surviving candidate events in data is shown in Fig. 1(a). Clear peaks from π^0 , η , and η' are observed in the $M(\gamma\gamma)$ spectrum, as shown in Fig. 1(b). To reject the backgrounds with $\pi^0 \rightarrow \gamma\gamma$, $\eta \rightarrow \gamma\gamma$, or $\eta' \rightarrow \gamma\gamma$ in the final state, events with $M(\gamma\gamma) \in (0.11, 0.16)$ GeV/ c^2 , $M(\gamma\gamma) \in (0.46, 0.59)$ GeV/ c^2 ,

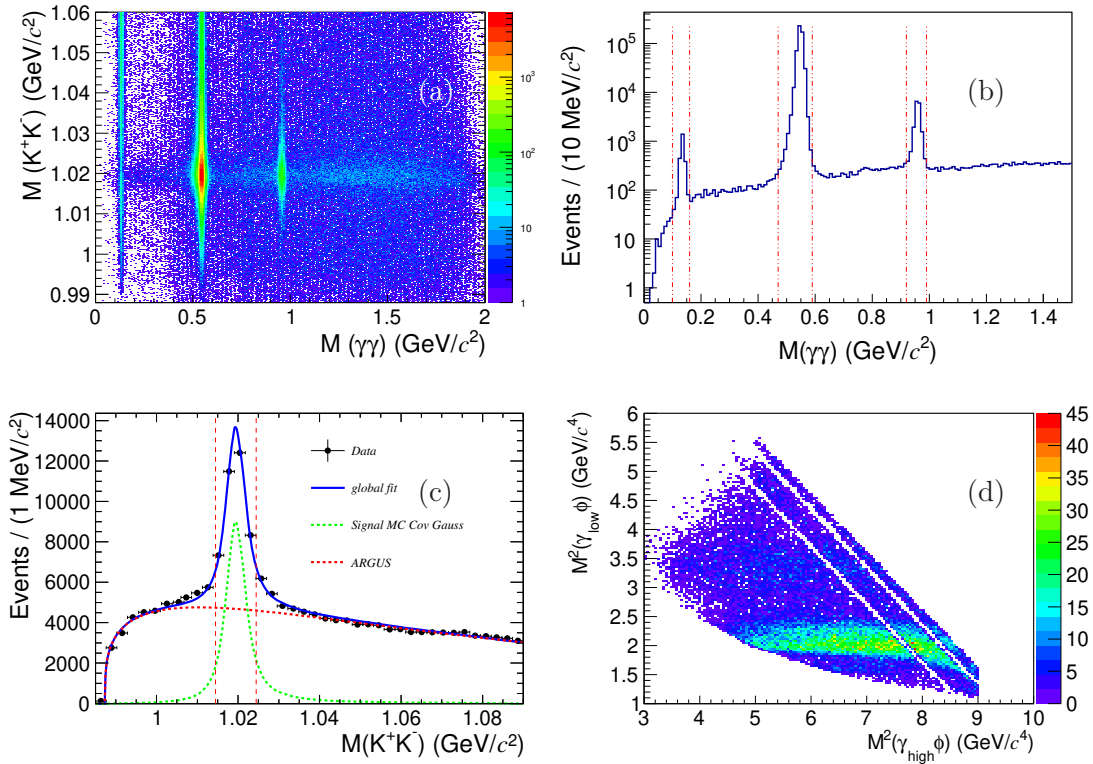


Figure 1: Distribution of (a) $M(\gamma\gamma)$ versus $M(K^+K^-)$, (b) $M(\gamma\gamma)$, pair of the red dashed vertical lines denote the π^0 , η and η' background regions. (c) $M(K^+K^-)$, dots with error bars are data, blue line denote global fit curve, green dash line denote signal shape, red dot-dash line is background shape, pair of the red dashed vertical lines denote the ϕ signal region. (d) Dalitz plot of $M^2(\gamma_{high}\phi)$ versus $M^2(\gamma_{low}\phi)$ with ϕ requirement of the accepted $J/\psi \rightarrow \gamma\gamma\phi$ candidates.

$M(\gamma\gamma) \in (0.92, 0.99)$ GeV/ c^2 , or $M^2(\gamma_{high}\phi) > 9$ GeV $^2/c^4$ are removed (here, γ_{low} and γ_{high} denote the photons with lower and higher energy in the $\gamma\gamma K^+K^-$ final state). Likewise, the $M(K^+K^-)$ spectrum is shown in Fig. 1(c). The ϕ candidates are selected by requiring $|M(K^+K^-) - M_\phi| < 0.005$ GeV/ c^2 , where M_ϕ is the nominal mass of the ϕ meson. From a one-dimensional fit to the $M(K^+K^-)$ distribution, the fractions of ϕ -events and non- ϕ events are determined to be 55.3% and 44.7% in the ϕ signal region, respectively. In the fit, the signal is modeled by an MC-simulated shape convolved with a Gaussian function describing the resolution difference between data and MC simulation. The background shape is described by an ARGUS function [33]. After applying the ϕ mass restrictions, the Dalitz plot of $M^2(\gamma_{high}\phi)$ versus $M^2(\gamma_{low}\phi)$ is shown in Fig. 1(d). Finally, 38383 events survive the event selection criteria.

4 Background Treatment

After the above event selections, the remaining backgrounds are categorized into two types, backgrounds without ϕ and backgrounds with ϕ .

4.1 Treatment of non- ϕ background

The dominant non- ϕ background components are mainly from $J/\psi \rightarrow \gamma X$ ($X = f_1(1285)$, $\eta(1405)$ and $f_1(1420)$), $X \rightarrow K^+K^-\pi^0$, leading to $\gamma K^+K^-\pi^0$ final states. It is difficult to distinguish the signal from these background components because the $M(K^+K^-)$ value from $X \rightarrow K^+K^-\pi^0$ is close to the K^+K^- mass threshold.

Based on the analysis of the signal-to-background ratio Q in a very small cell of the available phase space around each specific event, the quality factor method [32] is used to estimate the non- ϕ backgrounds. In this method, a distinct kinematic variable (ζ_r) characterizing the events is used to parameterize the shapes for both signal and background. For a specific event, a set of nearest neighbors (N_c) within the small cell of the available PHSP is selected. In order to measure distances between events, a collection of kinematic observables ($\vec{\zeta}$) that span the PHSP for the reaction is selected to define a metric. Using this metric, the distance between any two events, d_{ij} , is given as

$$d_{i,j}^2 = \sum_{k \neq r} \left[\frac{\zeta_k^i - \zeta_k^j}{\Delta_k} \right]^2, \quad (4.1)$$

where the sum is over all kinematic observables except ζ_r , and Δ_k is a normalization factor that represents the weights of the kinematic variable. Seven coordinates are used for the metric as listed in Table 1.

Table 1: Set of the kinematic observables ($\vec{\zeta}_k$) used for background subtraction.

$\vec{\zeta}_i$	Description	Δ_k
$\cos(\gamma_{\text{high}})$	Polar angle of high energy photon	2
$\cos(k)$	Polar angle of K^+ in the ϕ rest frame	2
$\cos(\phi)$	Polar angle of ϕ in X rest frame	2
$\phi(k)$	Azimuthal decay angle of K^+ in the ϕ rest frame	2π
$\phi(\phi)$	Azimuthal decay angle of ϕ in X rest frame	2π
$M^2(\gamma_{\text{low}}\phi)$	Squared invariant mass of $\gamma_{\text{low}}\phi$	$0.1 \text{ GeV}/c^2$
$M^2(\gamma_{\text{high}}\phi)$	Squared invariant mass of $\gamma_{\text{high}}\phi$	$0.15 \text{ GeV}/c^2$

In this analysis, $M(K^+K^-)$ is chosen as the distinct kinematic variable. The signal component is modeled as a convolution of a relativistic P-wave Breit-Wigner function and a Gaussian resolution function, while the background is described by an inverse ARGUS function [33]. The value of N_c is required to be as small as possible to ensure that the PHSP cell of all selected neighbors is small and that the background behaves smoothly within the cell. At the same time, N_c has to be large enough to ensure stable and reliable single-event fits.

The N_c events are then fitted using the unbinned maximum likelihood method to obtain estimators for the parameters of

$$f(\xi) = N \cdot [f_s \cdot S(\zeta) + (1 - f_s) \cdot B(\zeta)], \quad (4.2)$$

where $S(\zeta)$ and $B(\zeta)$ represent the probability density functions of signal and background, respectively, ξ is the selected kinematic variable, N denotes a normalization constant, and f_s describes a signal fraction with a value constrained within the range $[0.0, 1.0]$. The Q-value for each event is then given by

$$Q = \frac{f_s \cdot S(\zeta)}{f_s \cdot S(\zeta) + (1 - f_s) \cdot B(\zeta)}. \quad (4.3)$$

Here, Q and (1-Q) represent the probabilities of an event to be signal and background, respectively, these can be used as an event-weight to determine the contribution of the signal to a given physical distribution. Figure 2 shows the angular distributions and several invariant mass spectra for the selected events within the ϕ signal region, Q-weighted and (1-Q)-weighted.

The sum of all obtained Q-values (weights) is taken as the number of signal events, yielding 20453 events. All further analysis steps are performed using this weighted data sample.

4.2 Treatment of ϕ background

The dominant ϕ related background is $J/\psi \rightarrow \phi\pi^0\pi^0$, which includes a rich spectrum of intermediate resonances [34]. A multi-dimensional re-weighting method [35] is applied to the PHSP MC sample to obtain a “data-like” MC sample of $J/\psi \rightarrow \phi\pi^0\pi^0$. The weighted $J/\psi \rightarrow \phi\pi^0\pi^0$ MC events are subjected to the $J/\psi \rightarrow \gamma\gamma\phi$ event selection criteria. The surviving events are normalized according to the BF, resulting in 3155 background events which will be statistically subtracted in the PWA. Figure 3 shows the comparison of data and weighted PHSP MC sample for the selected $J/\psi \rightarrow \phi\pi^0\pi^0$ events. As can be seen from the plots, the data-MC consistencies are very good.

To estimate the other surviving background sources, exclusive MC samples of $J/\psi \rightarrow \phi\pi^0$, $J/\psi \rightarrow \phi\eta$, and $J/\psi \rightarrow \phi\eta'$ are generated with the angular distribution for J/ψ decays to a vector meson and a pseudoscalar meson. The surviving events are normalized according to the PDG BFs [1], resulting in 157 background events which also will be subtracted from the data by assigning negative weights to them in the PWA.

5 Partial Wave Analysis

Using the GPUPWA framework [36], a PWA is performed on the selected $\gamma\gamma\phi$, $\phi \rightarrow K^+K^-$ candidates to disentangle the structures in the Dalitz plot. The amplitudes in the sequential radiative decay $J/\psi \rightarrow \gamma X$, $X \rightarrow \gamma\phi$ are constructed using the covariant tensor amplitudes [37]. The decay amplitudes are written as

$$\begin{aligned} A &= \psi_\mu(p, m_\psi) \epsilon_\nu^*(q_1, m_\gamma) \epsilon_\alpha^*(q_2, m_{\gamma'}) A^{\mu\nu\alpha} \\ &= \psi_\mu(p, m_\psi) \epsilon_\nu^*(q_1, m_\gamma) \epsilon_\alpha^*(q_2, m_{\gamma'}) \sum_i \Lambda_i U_i^{\mu\nu\alpha}, \end{aligned} \quad (5.1)$$

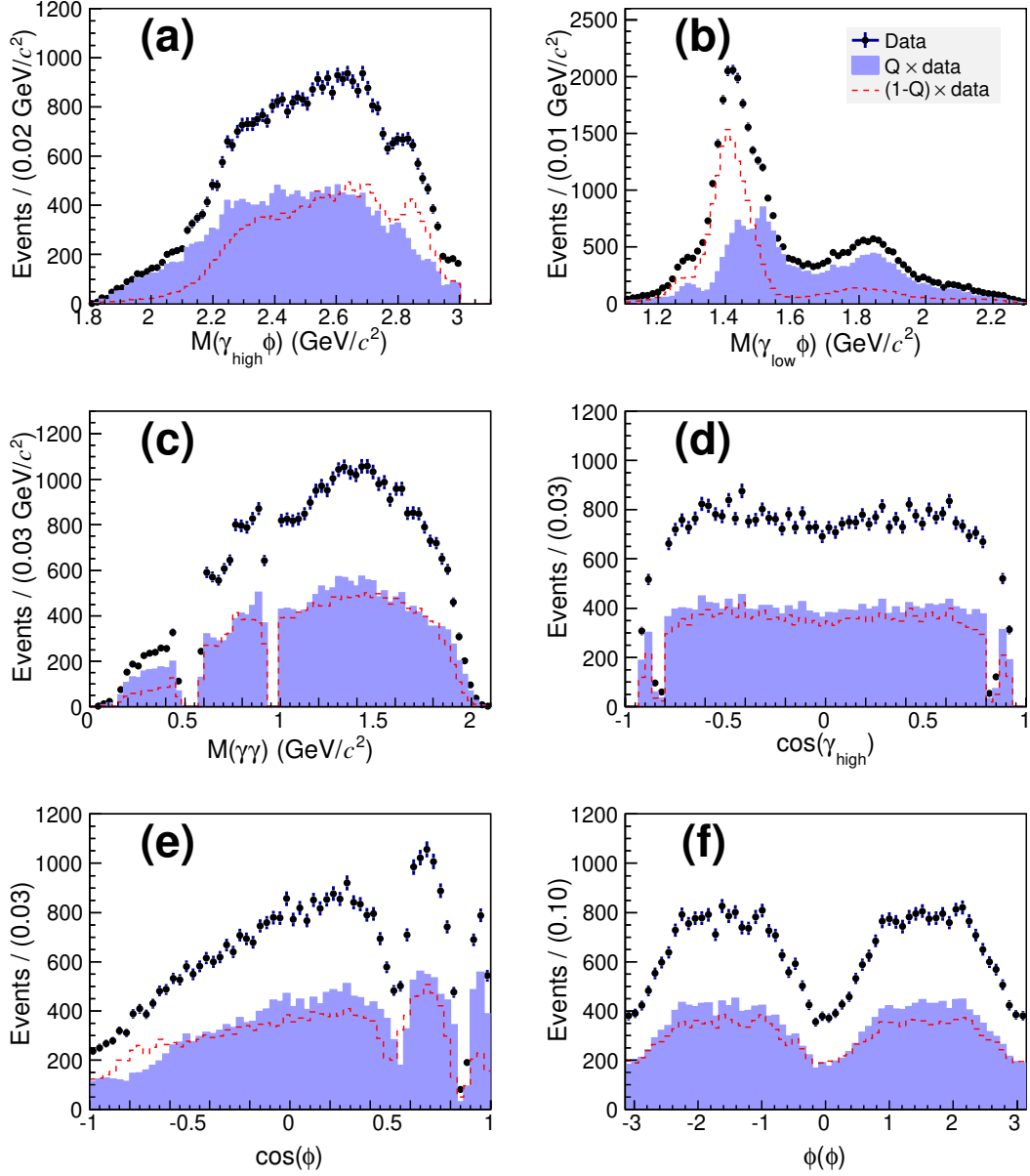


Figure 2: Distributions of (a) $M(\gamma_{\text{high}}\phi)$, (b) $M(\gamma_{\text{low}}\phi)$, (c) $M(\gamma\gamma)$, (d) $\cos(\gamma_{\text{high}})$, (e) $\cos(\phi)$, and (f) $\phi(\phi)$ of the accepted $J/\psi \rightarrow \gamma\gamma\phi$ candidates. The black dots with error bars are the selected events in the ϕ signal region without any weight, the purple histograms are Q -weighted data, and the red dashed lines are $(1 - Q)$ weighted data.

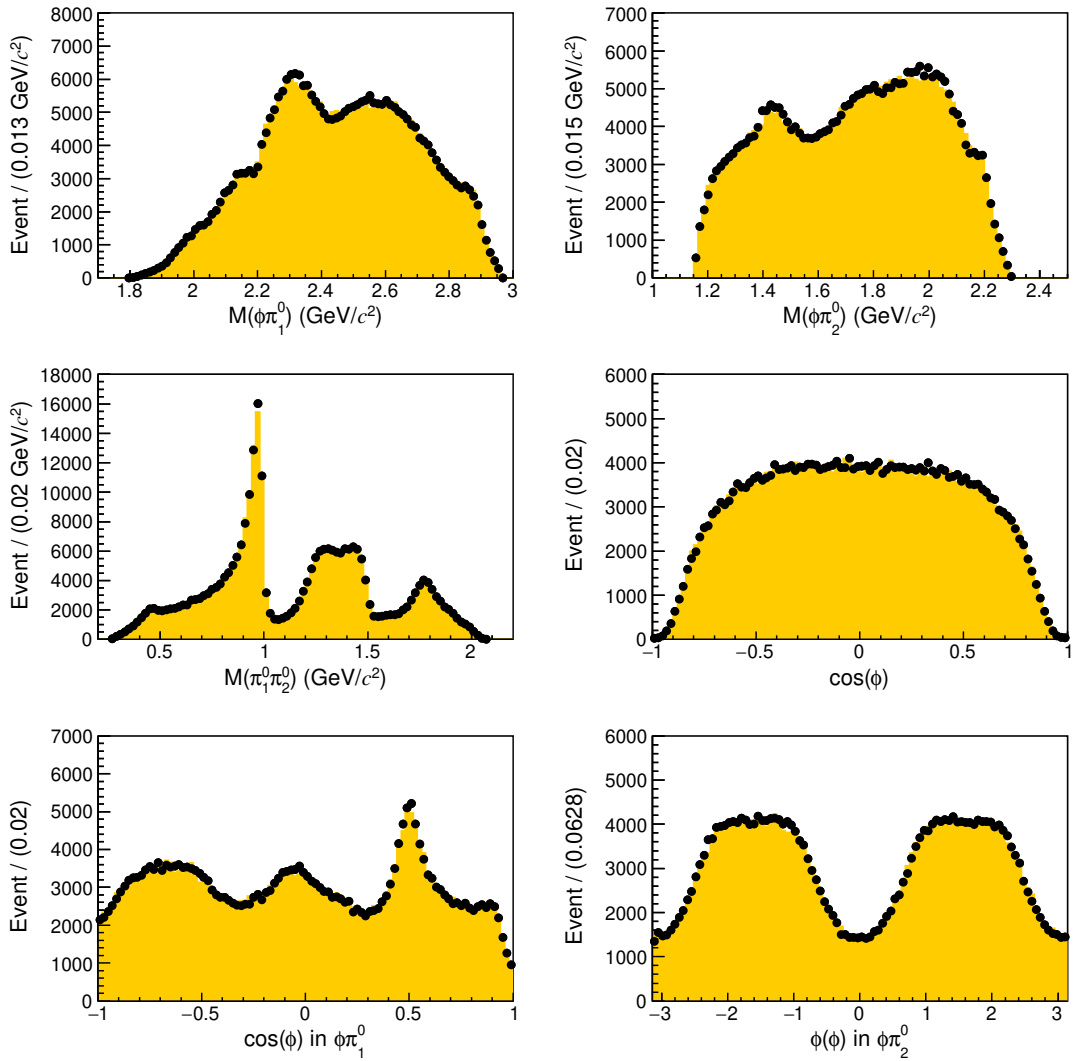


Figure 3: Comparison of data and weighted MC sample for $J/\psi \rightarrow \phi\pi^0\pi^0$. The dots with error bars are data, and the orange shadows are the weighted PHSP MC sample.

where the sum runs over the number of independent amplitudes. The $\psi_\mu(p, m_\psi)$ is the polarization four-vector for J/ψ , and $\epsilon_\nu^*(q_i, m_\gamma)$ ($i = 1, 2$) are the polarization four-vectors for the two photons; $U_i^{\mu\nu\alpha}$ is the i -th partial-wave amplitude, Λ_i is the complex coupling coefficient of the amplitude. The partial wave amplitudes U_i used in this analysis are constructed with the four-momenta of the particles in the final state, their specific expressions are given in Ref. [37].

In this analysis, the resonances are parameterized by a constant-width relativistic BW propagator,

$$BW(s) = \frac{1}{M^2 - s - iM\Gamma}, \quad (5.2)$$

where M and Γ are the mass and width of the intermediate resonance X , respectively; s is the invariant mass squared of $\gamma_i\phi$ system.

The complex coefficients of the amplitudes (relative magnitudes and phases) and the resonance parameters (masses and widths) are determined by an unbinned maximum likelihood fit to the data events. The likelihood is constructed following a method similar to the one used in Ref. [38].

The probability to observe the i -th event characterized by the measurement ξ_i , i.e., the measured four-momenta of the particles in the final state, is

$$P(\xi_i) = \frac{|M(\xi_i)|^2 \epsilon(\xi_i) \Phi(\xi_i)}{\sigma'}, \quad (5.3)$$

where $\epsilon(\xi_i)$ is the detection efficiency, $\Phi(\xi_i)$ is the standard element of PHSP, $M(\xi_i) = \sum_X A_X(\xi_i)$ is the matrix element describing the decay $J/\psi \rightarrow \gamma\gamma\phi$, $A_X(\xi_i)$ is the amplitude corresponding to the intermediate resonance X , and $\sigma' \equiv \int |M(\xi)|^2 \epsilon(\xi) \Phi(\xi) d\xi$ is the normalization integral.

The joint likelihood for observing N events in the data sample is then given by

$$\mathcal{L} = \prod_{i=1}^N \frac{|M(\xi_i)|^2 \epsilon(\xi_i) \Phi(\xi_i)}{\sigma'}. \quad (5.4)$$

The fit minimizes the negative log-likelihood (NLL) value

$$-\ln \mathcal{L} = -\sum_{i=1}^N \ln |M(\xi_i)|^2 + N \ln \sigma' - \sum_{i=1}^N \ln \epsilon(\xi_i) \Phi(\xi_i), \quad (5.5)$$

where the third term is a constant with no impact on the determination of the fit parameters and therefore is not considered in the fit.

The free parameters are optimized by MINUIT [39]. The normalization integral σ' is evaluated using MC simulation with importance sampling [40, 41]. The MC sample of N_{gen} is generated with signal events distributed uniformly in PHSP. These events are simulated by taking into account of detector response, and subjected to the same selection criteria of data, yielding a sample of N_{acc} accepted events. The normalization integral is computed as

$$\sigma' = \int |M(\xi)|^2 \epsilon(\xi) \Phi(\xi) d\xi \propto \frac{1}{N_{\text{gen}}} \sum_j^{N_{\text{acc}}} |M(\xi_j)|^2, \quad (5.6)$$

where the constant value of the PHSP integral $\int \Phi(\xi) d\xi$ is ignored.

While the contribution from the non- ϕ background is taken into account by the Q -factor method, the ϕ background is subtracted in the NLL calculation. Thus, the NLL is given by

$$-\ln \mathcal{L} = -\left[\ln \mathcal{L}_{\text{Qweighted data}} - \sum \ln(\mathcal{L}_{\phi\pi^0\pi^0} + \mathcal{L}_{\phi\pi^0} + \mathcal{L}_{\phi\eta} + \mathcal{L}_{\phi\eta'}) \right]. \quad (5.7)$$

The log-likelihood is scaled by taking into account the statistical uncertainties of subtracted backgrounds [42].

The fitted event yield N_X for an intermediate resonance X is determined as

$$N_X = \frac{\sigma_X}{\sigma'} \cdot N, \quad (5.8)$$

where N is the number of selected events after background subtraction, and

$$\sigma_X = \frac{1}{N_{\text{gen}}} \sum_j^{N_{\text{acc}}} |A_X(\xi_j)|^2 \quad (5.9)$$

is calculated with the same MC sample as the normalization integral σ' .

The detection efficiency ϵ_X for an intermediate resonance X is obtained by the partial wave amplitude weighted MC sample,

$$\epsilon_X = \frac{\sum_j^{N_{\text{acc}}} |A_X(\xi_j)|^2}{\sum_n^{N_{\text{gen}}} |A_X(\xi_n)|^2}. \quad (5.10)$$

Finally, the BF of $J/\psi \rightarrow \gamma X, X \rightarrow \gamma\phi$ is calculated by

$$\mathcal{B}(J/\psi \rightarrow \gamma X \rightarrow \gamma\phi) = \frac{N_X}{N_{J/\psi} \cdot \epsilon_X \cdot \mathcal{B}(\phi \rightarrow K^+K^-)}. \quad (5.11)$$

6 PWA Results

In this analysis, all kinematically-allowed resonances with $J^{PC} = 0^{++}, 0^{-+}, 1^{++}, 1^{-+}, 2^{++}$ and 2^{-+} listed in the PDG [1] are taken into account. Moreover, an exotic structure $\eta_1(1855)$ recently observed in $J/\psi \rightarrow \gamma\eta\eta'$ by BESIII [43, 44] and a glueball candidate $X(2370)$ observed in $J/\psi \rightarrow \gamma\pi^+\pi^-\eta'$ [15] are also considered. Non-resonant contributions, described by 0^{++} PHSP, 0^{-+} PHSP, 1^{++} PHSP, 2^{++} PHSP, or 2^{-+} PHSP, are also taken into account. All possible resonances listed in Table 2 are considered and their statistical significances are evaluated. Only the components with a statistical significance greater than 5σ are kept in the baseline solution. The statistical significance for each resonance is determined from the relative changes of optimal NLL values when including and excluding it in the fit, assuming the χ^2 distribution hypothesis and taking into account the change in the number of degrees of freedom.

Ten resonances are kept in the baseline set of amplitudes. By optimizing the masses and widths of these resonances we identify them as $f_1(1285)$, $f_1(1420)$, $\eta(1405)$, $f_1(1510)$, $f_2(1525)$, $X(1835)$, $f_2(1950)$, $f_2(2010)$, $f_0(2200)$, and η_c . Columns 2 and 3 of Table 3 show the results of the fit in which masses and widths of all resonances are optimized simultaneously (see optimization plots in the Appendix). To improve the fit stability, we perform a ‘‘baseline fit’’ in which masses and widths of all resonances except $\eta(1405)$ and $X(1835)$ are fixed to the PDG values. The results of the baseline fit, which we consider more reliable, are listed in columns 4, 5, 6 and 7 in Table 3. The baseline results show that the structure in the vicinity of $1.4 \text{ GeV}/c^2$, as shown in Fig. 4(a), needs to be described by $\eta(1405)$ and $f_1(1420)$ in the $\gamma\phi$ system. The measured mass and width for $\eta(1405)$ are $1422.3 \pm 2.1_{-7.1}^{+4.3} \text{ MeV}/c^2$ and $86.3 \pm 2.7_{-17.1}^{+3.7} \text{ MeV}$, respectively. The spin-parity of the structure with mass around $1.8 \text{ GeV}/c^2$ is determined to be 0^{-+} . Its mass and width are measured to be $1849.3 \pm 3.0_{-10.0}^{+5.4} \text{ MeV}/c^2$ and $179.6 \pm 8.7_{-24.9}^{+15.9} \text{ MeV}$, which are consistent with those of the $X(1835)$ measured in $J/\psi \rightarrow \gamma K_S^0 K_S^0 \eta$ [45]. Changing the J^{PC} in the baseline set of amplitudes to other hypotheses results in a worse negative log-likelihood by

Table 2: Pool of candidate resonances for the PWA.

0^{++}	0^{-+}	1^{++}	1^{-+}	2^{++}	2^{-+}
$f_0(1500)$	$\eta(1295)$	$f_1(1285)$	$\eta_1(1855)$	$f_2(1270)$	$\eta_2(1645)$
$f_0(1710)$	$\eta(1405)$	$f_1(1420)$		$f_2(1525)$	$\eta_2(1870)$
$f_0(1760)$	$\eta(1475)$	$f_1(1510)$		$f_2(1565)$	
$f_0(2020)$	$\eta(1760)$			$f_2(1640)$	
$f_0(2100)$	$X(1835)$			$f_2(1810)$	
$f_0(2200)$	$\eta(2225)$			$f_2(1910)$	
$f_0(2330)$	$X(2370)$			$f_2(1950)$	
	η_c			$f_2(2010)$	
				$f_2(2150)$	
				$f_2(2340)$	

at least 13.2 units. Specifically, when the J^{PC} assignment of the $f_1(1420)$, $\eta(1405)$, and $X(1835)$ change to other hypotheses, it results in an increase NLL by at least 14.6, 79.7, and 45.9, respectively. The fit fractions of each component and their interference fractions are shown in Table 4. The comparisons between the data and the PWA fit projections for the distributions of $M(\gamma_{low}\phi)$, $M(\gamma_{high}\phi)$, $M(\gamma\gamma)$ and several angular distributions are shown in Fig. 4. The χ^2/N_{bin} is displayed on each figure to demonstrate the goodness of fit, where N_{bin} is the number of bins in each histogram, and χ^2 is defined as:

$$\chi^2 = \sum_{i=1}^{N_{\text{bin}}} \chi^2 = \sum_{i=1}^{N_{\text{bin}}} \frac{(n_i - \nu_i)^2}{\nu_i^2}, \quad (6.1)$$

where n_i and ν_i are the number of events for the data and the fit projections with the baseline set of amplitudes in the i th bin of each figure, respectively.

All other possible resonances have a statistical significance less than 5σ when added to the baseline set of amplitudes. In addition, the statistical significances of all possible non-resonant contributions are also less than 5σ , as shown in Table 5. Among them, the $f_0(2020)$ has a significance of 4.9σ , but its fit fraction is much less than 1%. The impact of the inclusion of $f_0(2020)$ on the PWA result is assigned as a systematic uncertainty, as discussed in Section VI. To investigate additional possible contributions, resonances with different J^{PC} (0^{++} , 0^{-+} , 1^{++} , 1^{-+} , 2^{++} , 2^{-+}) and different masses and widths are added to the baseline set of amplitudes. No significant contribution is found.

A further check on the pseudoscalar structure with a mass around $1.4 \text{ GeV}/c^2$ is performed. If the mass and width of the pseudoscalar state are fixed to the PDG values of $\eta(1405)$ or $\eta(1475)$ [1], the log-likelihood worsens by 45.6 or 56.2. Another test includes an additional $\eta(1475)$ with parameters fixed at the PDG values or free resonance parameters in the baseline model, the statistical significances of these contributions are 2.3σ and 3.9σ . These results indicate that only one pseudoscalar state is needed in the vicinity of $1.4 \text{ GeV}/c^2$.

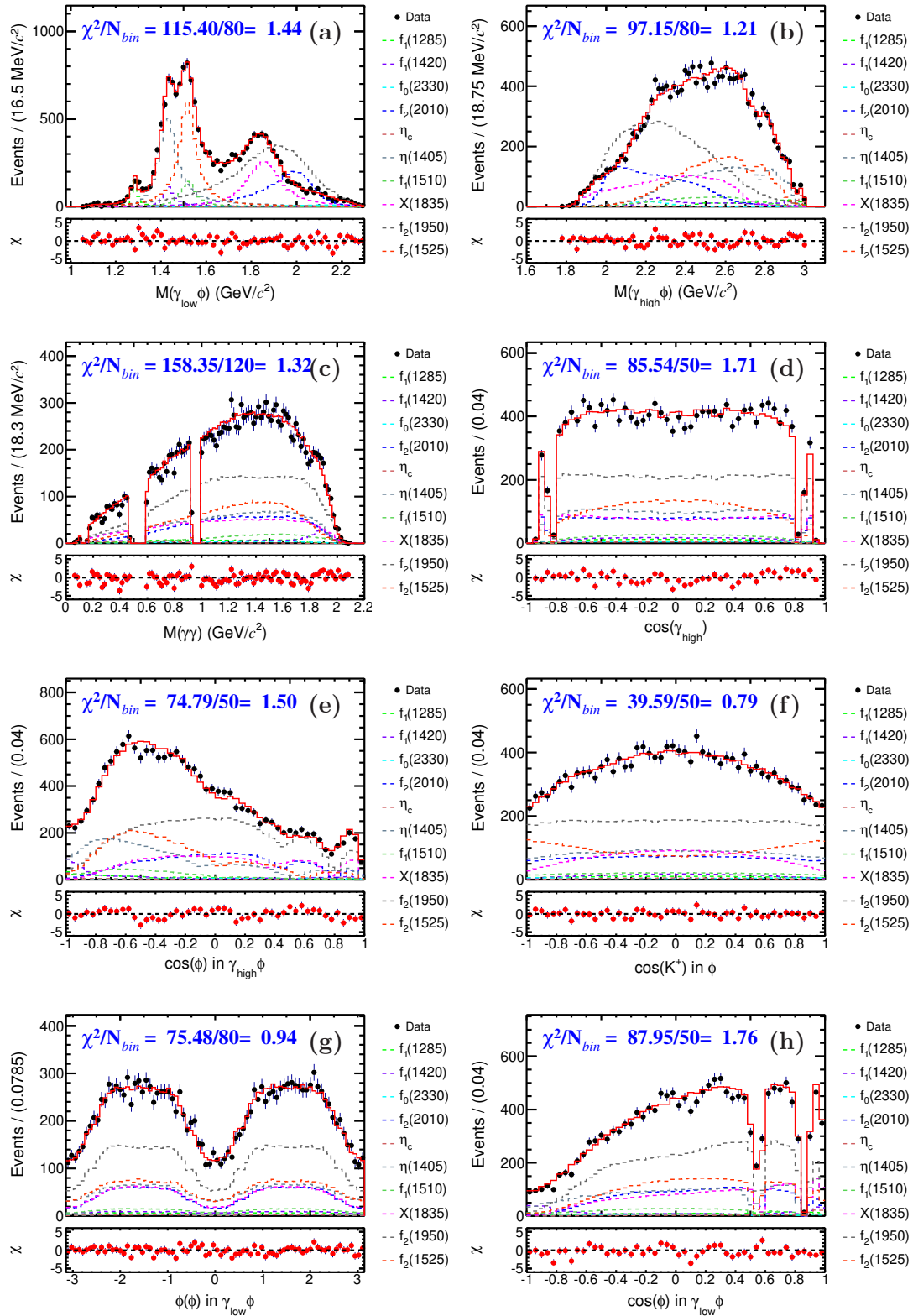


FIG. 4: PWA fit projections on (a) $M(\gamma_{low}\phi)$, (b) $M(\gamma_{high}\phi)$, (c) $M(\gamma\gamma)$ and the angular distributions of $J/\psi \rightarrow \gamma\gamma\phi$, (d) $\cos(\theta)$ of the radiative γ , (e) $\cos(\theta)$ of ϕ in the $\gamma_{high}\phi$ rest frame, (f) $\cos(\theta)$ of K^+ in the ϕ rest frame, (g) azimuthal angle of ϕ in the X rest frame, and (h) $\cos(\theta)$ of ϕ in the $\gamma_{low}\phi$ rest frame. Black dots with error bars represent data and red lines represent the projections of global fit. Dashed lines represent contributions of each component in the baseline solution.

Table 3: The masses and widths for resonances, the BFs of $\mathcal{B}(J/\psi \rightarrow \gamma X \rightarrow \gamma\gamma\phi)$, and the statistical significances obtained from the PWA. Columns 2 and 3 are the results of the simultaneous optimization of all resonances with statistical uncertainties. Columns 4, 5, 6 and 7 are the baseline fit results with the statistical and systematic uncertainties after fixing the masses and widths of the f -states and η_c to the PDG values [1].

Resonance	M (MeV/ c^2)	Γ (MeV)	M (MeV/ c^2)	Γ (MeV)	$\mathcal{B}(\times 10^{-6})$	Significance
$f_1(1285)$	1281 ± 2.0	26 ± 3	1281.9	22.7	$0.29 \pm 0.03^{+0.11}_{-0.09}$	17.3σ
$f_1(1420)$	$1425^{+1.9}_{-2.2}$	$61^{+3.5}_{-4.0}$	1426.3	54.5	$0.55 \pm 0.07^{+0.18}_{-0.17}$	9.0σ
$\eta(1405)$	$1422^{+1.0}_{-3.0}$	86 ± 3.0	$1422.0 \pm 2.1^{+5.9}_{-7.8}$	$86.3 \pm 2.7^{+6.6}_{-17.4}$	$3.57 \pm 0.18^{+0.59}_{-0.61}$	18.9σ
$f_1(1510)$	$1517^{+1.9}_{-2.8}$	71 ± 5.0	1518.0	73.0	$0.78 \pm 0.09^{+0.34}_{-0.30}$	5.3σ
$f_2(1525)$	$1518^{+0.9}_{-1.8}$	$85^{+2.5}_{-4.0}$	1517.4	86.0	$2.76 \pm 0.18^{+0.90}_{-0.61}$	16.4σ
$X(1835)$	$1855^{+2.5}_{-3.0}$	$181^{+6.0}_{-7.0}$	$1849.3 \pm 3.0^{+7.6}_{-10.0}$	$179.6 \pm 8.7^{+22.5}_{-27.9}$	$3.37 \pm 0.19^{+0.78}_{-1.10}$	15.3σ
$f_2(1950)$	$1938^{+5.0}_{-4.0}$	475 ± 10.0	1936.0	464.0	$9.96 \pm 0.60^{+3.44}_{-2.13}$	13.1σ
$f_2(2010)$	$2012^{+2.1}_{-3.5}$	$202^{+6.0}_{-6.5}$	2011.0	202.0	$4.63 \pm 0.43^{+1.42}_{-1.46}$	11.3σ
$f_0(2200)$	2214 ± 12.0	209^{+34}_{-30}	2187.0	207.0	$0.20 \pm 0.04^{+0.05}_{-0.07}$	6.3σ
η_c	$2981 \pm^{+1.5}_{-2.5}$	$25^{+2.5}_{-3.0}$	2983.9	32.0	$0.21 \pm 0.03^{+0.05}_{-0.07}$	12.9σ

Table 4: Fit fractions of each component and interference fractions between two components in the baseline solution. The uncertainties are statistical only. All the values are given in %.

Resonance	$f_1(1285)$	$f_1(1420)$	$\eta(1405)$	$f_1(1510)$	$f_2(1525)$	$X(1835)$	$f_2(1950)$	$f_2(2010)$	$f_0(2200)$	η_c
$f_1(1285)$	1.84 ± 0.16	0.54 ± 0.11	0.34 ± 0.08	-0.26 ± 0.11	-0.31 ± 0.04	-0.34 ± 0.09	-0.14 ± 0.07	-0.09 ± 0.05	0.00 ± 0.00	0.07 ± 0.03
$f_1(1420)$		3.94 ± 0.42	-0.30 ± 0.21	-2.38 ± 0.45	-0.16 ± 0.22	1.00 ± 0.18	-3.42 ± 0.32	2.45 ± 0.22	0.00 ± 0.00	-0.18 ± 0.05
$\eta(1405)$			21.85 ± 0.79	-0.78 ± 0.17	-0.29 ± 0.09	2.14 ± 0.82	-0.19 ± 0.09	-0.14 ± 0.05	0.02 ± 0.01	1.66 ± 0.16
$f_1(1510)$				5.62 ± 0.56	0.55 ± 0.42	0.17 ± 0.16	4.85 ± 0.45	-3.10 ± 0.27	-0.13 ± 0.05	-0.13 ± 0.05
$f_2(1525)$					18.74 ± 0.95	0.09 ± 0.06	7.83 ± 0.96	-2.14 ± 0.45	0.18 ± 0.06	-0.12 ± 0.01
$X(1835)$						19.03 ± 0.76	1.88 ± 0.17	-1.12 ± 10.13	0.00 ± 0.00	-2.13 ± 0.14
$f_2(1950)$							60.94 ± 2.78	-72.11 ± 4.56	-1.06 ± 0.21	0.24 ± 0.04
$f_2(2010)$								19.03 ± 0.76	1.85 ± 0.26	-0.14 ± 0.02
$f_0(2200)$									30.78 ± 2.45	0.01 ± 0.00
η_c										1.28 ± 0.14

The PWA result shows that there is no evidence for the $\eta(1295)$, $\eta(1475)$, $\eta_1(1855)$, and $X(2370)$ in the $\gamma\phi$ system. The same approach as in Ref. [46] is used to determine the upper limits for the production of these four states. The systematic uncertainties for these upper limits are calculated with same method as for the baseline solution, cf. Sec. 7, and are summed in quadrature with the statistical uncertainty for each respective yield. The resulting uncertainty is used to determine the 90% confidence level deviation, and added to the "updated nominal" yield of the candidate state to obtain the corresponding upper limit for the BFs $\mathcal{B}(J/\psi \rightarrow \gamma\eta(1295) \rightarrow \gamma\gamma\phi)$, $\mathcal{B}(J/\psi \rightarrow \gamma\eta(1475) \rightarrow \gamma\gamma\phi)$, $\mathcal{B}(J/\psi \rightarrow \gamma\eta_1(1855) \rightarrow \gamma\gamma\phi)$, and $\mathcal{B}(J/\psi \rightarrow \gamma X(2370) \rightarrow \gamma\gamma\phi)$.

Table 5: Changes in the negative log-likelihood ($\Delta \ln \mathcal{L}$) and in the number of free parameters (Δdof) by considering additional resonances and the corresponding statistical significance.

Resonance	$\Delta \ln \mathcal{L}$	Δdof	Significance
$\eta(1295)$	0.1	2	0.1σ
$f_2(1270)$	3.9	18	0.1σ
$\eta(1475)$	8.6	2	3.7σ
$f_0(1500)$	0.8	2	0.7σ
$f_2(1565)$	12.4	18	1.5σ
$f_2(1640)$	7.4	18	0.4σ
$\eta_2(1645)$	3.3	18	0.0σ
$f_0(1710)$	2.7	2	1.8σ
$\eta(1760)$	0.6	2	0.6σ
$f_2(1810)$	10.3	18	1.0σ
$f_2(1910)$	9.6	18	0.9σ
$\eta_1(1855)$	2.9	8	0.4σ
$f_0(2020)$	13.6	2	4.9σ
$f_0(2100)$	7.4	2	3.4σ
$f_2(2150)$	9.6	18	0.9σ
$\eta(2225)$	0.6	2	0.6σ
$f_0(2330)$	12.0	2	4.5σ
$f_2(2340)$	15.2	18	2.1σ
$X(2370)$	0.4	2	0.4σ
0^{++} PHSP	0.9	2	0.9σ
0^{-+} PHSP	4.1	2	2.4σ
1^{++} PHSP	5.9	8	1.5σ
2^{++} PHSP	18.4	18	2.8σ
2^{-+} PHSP	5.9	18	0.2σ

7 Systematic Uncertainties

7.1 Systematic uncertainties due to the event selections

The systematic uncertainties that arise from event selection impact the BF measurements. The sources contributing to the uncertainty are listed below.

- (i) Total number of J/ψ events. The uncertainty due to the total number of J/ψ events is determined to be 0.43% according to Ref. [47].
- (ii) Kaon tracking and PID. The charged kaon tracking and PID efficiencies are studied using control sample $J/\psi \rightarrow K_S^0 K \pi$, $K_S^0 \rightarrow \pi^+ \pi^-$ [48]. The systematic uncertainty

from tracking or PID efficiencies is estimated to be 1% per kaon.

- (iii) Photon detection efficiency. The photon detection efficiency is studied using $J/\psi \rightarrow \rho\pi^0 \rightarrow \pi^+\pi^-\pi^0$ [49] control sample. The systematic uncertainty of photon detection efficiency is assigned to be 1% per photon.
- (iv) Kinematic fit. The track helix parameter correction method [50] is used to investigate the systematic uncertainty associated with the 4C kinematic fit. The difference in the detection efficiencies with and without the helix correction, 1.2%, is taken as the systematic uncertainty.

The total systematic uncertainty from event selection is determined to be 3.5%, obtained as a quadratic sum of the contributions discussed above.

7.2 Systematic uncertainties due to the PWA

Systematic uncertainty from the PWA impacts both branching fractions and resonance parameters. The sources of this uncertainty are described below.

- (i) Mass window cuts. Uncertainties from mass window requirements of π^0 , η , and η' are estimated by enlarging or shrinking each mass window within 2 MeV/ c^2 . The largest changes in the measured masses and widths of $\eta(1405)$, $X(1835)$ and the BFs are assigned as the systematic uncertainties.
- (ii) Uncertainty from the non- ϕ backgrounds. Uncertainty due to the Q -factor method is obtained by smearing the nominal Q -value in each event by a Gaussian distribution with standard deviation

$$\sigma_Q^2 = \sum_{ij} \frac{\partial Q}{\partial \alpha_i} (C_\alpha^{-1})_{ij} \frac{\partial Q}{\alpha_j}, \quad (7.1)$$

where Q is the Q -factor, α_i are measurable quantities and C_α is the full covariance matrix. The new Q -factors are used in the PWA, and the differences between the nominal fit and the new fit are assigned as the systematic uncertainties.

- (iii) Uncertainty from the ϕ backgrounds : The “data-like” MC distributions of $J/\psi \rightarrow \phi\pi^0\pi^0$ have been obtained using a machine learning-based multi-dimensional reweighting method [35]. The systematic uncertainties can be estimated by changing the training features of machine learning. The training features are changed from four-momenta of final π_1^0 , π_2^0 and ϕ , $M(\phi\pi_1^0)$, $M(\phi\pi_2^0)$, $M(\pi_1^0\pi_2^0)$, $\cos(\phi)$, $\cos(\pi_1^0)$, and $\cos(\pi_2^0)$ to $P_z(\pi_1^0)$, $E(\pi_1^0)$, $P_z(\pi_2^0)$, $E(\pi_2^0)$, $P_z(\phi)$, $E(\phi)$, $M(\phi\pi_1^0)$, $M(\phi\pi_2^0)$, $M(\pi_1^0\pi_2^0)$, $\Phi(\phi)$, $\Phi(\pi_1^0)$, and $\Phi(\pi_2^0)$. The changes in the results are regarded as the systematic uncertainties. Since the remaining contributions of $J/\psi \rightarrow \phi\pi^0$, $J/\psi \rightarrow \phi\eta$, and $J/\psi \rightarrow \phi\eta'$ are small ($\sim 0.8\%$), their impact on the PWA results is considered as negligible.
- (iv) Uncertainties from resonance parameters : In the baseline solution, the resonance parameters of $f_1(1285)$, $f_1(1420)$, $f_2(2010)$, $f_0(2200)$, $f_1(1510)$, $f_2(1950)$, $f_2(1525)$, and η_c are fixed to the PDG [1] values. Alternative fits are performed with these

resonance parameters varied within one standard deviation of individual PDG value. The changes in the results are taken as the corresponding systematic uncertainties.

- (v) Uncertainties from additional resonances : Uncertainties arising from possible additional resonances are estimated by adding the $f_0(2020)$, $\eta(1405)$, 1^{++} PHSP, 2^{++} PHSP, or $\eta_2(1870)$ into the baseline fit individually. These candidate resonances are the most significant additional resonances for each possible J^{PC} . The resulting changes in the measurements are assigned as systematic uncertainties.

For each measurement, the individual uncertainties are assumed to be independent and are added in quadrature to obtain the total systematic uncertainty. The sources of systematic uncertainties for the measurements of masses and widths of $\eta(1405)$ and $X(1835)$ are summarized in Table 6. The relative systematic uncertainties for the BF measurements are summarized in Table 7.

Table 6: Systematic uncertainties on the masses and widths of $\eta(1405)$ and $X(1835)$. The systematic uncertainty introduced by $f_0(2020)$, which has a significance of 4.9σ , is explicitly denoted within parentheses.

Source	$\eta(1405)$		$X(1835)$	
	ΔM (MeV/ c^2)	$\Delta\Gamma$ (MeV/ c^2)	ΔM (MeV/ c^2)	$\Delta\Gamma$ (MeV/ c^2)
π^0 mass window cut	2.5	2.7	3.1	9.4
η mass window cut	2.0	3.0	1.0	8.8
η' mass window cut	1.6	1.9	0.5	2.6
Q -factor method	2.0	1.9	0.4	9.4
Multi-dimensional reweighting method	2.5	2.7	3.1	8.9
Resonance parameters	2.0	2.7	3.0	8.6
Extra resonances	$^{+2.8}_{-5.8}$ (+2.8)	$^{+2.2}_{-16.3}$ (-0.95)	$^{+5.4}_{-8.4}$ (-3.4)	$^{+9.7}_{-19.1}$ (-10.5)
Total	$^{+5.9}_{-7.8}$	$^{+6.6}_{-17.4}$	$^{+7.6}_{-10.0}$	$^{+22.5}_{-27.9}$

8 Summary and Discussion

In summary, based on a sample of $(10.09 \pm 0.04) \times 10^9$ J/ψ events collected with the BESIII detector, a PWA of the decay $J/\psi \rightarrow \gamma\gamma\phi$ is performed for the first time. The PWA result shows that the $J/\psi \rightarrow \gamma X, X \rightarrow \gamma\phi$ process has predominantly 2^{++} components. The decays of $\eta(1405)$, $X(1835)$, several f -states, and η_c into $\gamma\phi$ are observed with a statistical significance greater than 5σ . The mass and width optimizations of all the states are performed and the f -states are associated with $f_1(1285)$, $f_1(1420)$, $f_1(1510)$, $f_2(1525)$, $f_2(1950)$, $f_2(2010)$, and $f_0(2200)$. The decays of $f_1(1285)$, $f_1(1420)$, $\eta(1405)$, and $X(1835)$ to the $\gamma\phi$ final state have been confirmed, while the decays of the other resonances to the $\gamma\phi$ final state have been observed for the first time. The structure with mass around 1.4 GeV/ c^2 in $\gamma\phi$ system is due to the contributions of $\eta(1405)$ and $f_1(1420)$. The mass,

Table 7: Relative systematic uncertainties on $\mathcal{B}(J/\psi \rightarrow \gamma X \rightarrow \gamma\gamma\phi)$ (%). The systematic uncertainty introduced by $f_0(2020)$, which has a significance of 4.9σ , is explicitly denoted within parentheses.

Source	$f_1(1285)$	$f_1(1420)$	$f_0(2200)$	$f_2(2010)$	$\eta(2983)$	$\eta(1405)$	$f_1(1510)$	$X(1835)$	$f_2(1950)$	$f_2(1525)$
Event selection	3.5	3.5	3.5	3.5	3.5	3.5	3.5	3.5	3.5	3.5
π^0 mass window cut	10.7	6.6	6.3	13.7	11.8	6.2	8.5	12.1	9.2	7.1
η mass window cut	7.1	5.2	5.3	19.8	9.6	6.1	12.1	8.5	3.1	3.6
η' mass window cut	13.7	11.3	9.3	7.1	11.8	0.3	19.8	9.1	8.5	4.7
Q-factor method	12.7	14.1	6.6	4.7	6.8	1.9	17.7	8.8	1.4	7.2
Machine learning	15.2	13.8	6.5	6.6	9.3	0.9	7.7	3.9	4.8	11.2
Resonance parameters	12.2	6.5	4.7	6.5	0.9	7.1	15.0	0.5	15.2	11.3
Extra resonances	$^{+23.7}_{-3.4}$ (+17.6)	$^{+20.7}_{-17.1}$ (+9.8)	$^{+17.8}_{-28.5}$ (+17.8)	$^{+13.7}_{-15.7}$ (-7)	$^{+0.0}_{-24.7}$ (-13.3)	$^{+12.4}_{-11.7}$ (+6.1)	$^{+25.3}_{-17.0}$ (+6.2)	$^{+11.7}_{-26.8}$ (-14.4)	$^{+27.6}_{-4.9}$ (+16.6)	$^{+25.9}_{-3.2}$ (+6.3)
Total	$^{+38.3}_{-30.3}$	$^{+32.7}_{-30.6}$	$^{+24.4}_{-33.0}$	$^{+30.6}_{-31.6}$	$^{+22.7}_{-33.5}$	$^{+17.2}_{-16.7}$	$^{+43.1}_{-38.8}$	$^{+23.3}_{-33.5}$	$^{+34.6}_{-21.4}$	$^{+32.7}_{-22.1}$

width and product of BF of $\eta(1405)$ are measured to be $M = 1422.0 \pm 2.1^{+5.9}_{-7.8}$ MeV/ c^2 , $\Gamma = 86.3 \pm 2.7^{+6.6}_{-17.4}$ MeV and $\mathcal{B}(J/\psi \rightarrow \gamma\eta(1405) \rightarrow \gamma\gamma\phi) = (3.57 \pm 0.18^{+0.59}_{-0.61}) \times 10^{-6}$, respectively. The J^{PC} of $X(1835)$ is confirmed to be 0^{-+} . The mass, width and product of BF of $X(1835)$ are determined to be $1849.3 \pm 3.0^{+7.6}_{-10.0}$ MeV/ c^2 , $179.6 \pm 8.7^{+22.5}_{-27.9}$ MeV and $\mathcal{B}(J/\psi \rightarrow \gamma X(1835) \rightarrow \gamma\gamma\phi) = (3.37 \pm 0.19^{+0.78}_{-1.10}) \times 10^{-6}$, respectively. The observation of the $X(1835)$ decaying into $\gamma\phi$ final state indicates that this resonance also contains a sizable $s\bar{s}$ component.

The $\eta_c \rightarrow \gamma\phi$ decay is observed in the $\gamma\phi$ system for the first time, with a product BF of $\mathcal{B}(J/\psi \rightarrow \gamma\eta_c \rightarrow \gamma\gamma\phi) = (2.08 \pm 0.26^{+0.47}_{-0.70}) \times 10^{-7}$. This result provides new information to understand the properties of η_c .

No significant signals for $\eta(1295)$, $\eta(1475)$, $\eta_1(1855)$ and $X(2370)$ are observed in the $\gamma\phi$ system. The upper limits on the product BFs at the 90% confidence level are determined to be $\mathcal{B}(J/\psi \rightarrow \gamma\eta(1295) \rightarrow \gamma\gamma\phi) < 8.37 \times 10^{-7}$, $\mathcal{B}(J/\psi \rightarrow \gamma\eta(1475) \rightarrow \gamma\gamma\phi) < 3.80 \times 10^{-7}$, $\mathcal{B}(J/\psi \rightarrow \gamma\eta_1(1855) \rightarrow \gamma\gamma\phi) < 4.74 \times 10^{-6}$, and $\mathcal{B}(J/\psi \rightarrow \gamma X(2370) \rightarrow \gamma\gamma\phi) < 1.08 \times 10^{-7}$. The measured upper limit of $X(2370)$ is consistent with the prediction for a pseudoscalar glueball [51]. Moreover, the measured upper limit of $\eta_1(1855)$ is consistent with the radiative decay rate in Ref. [44].

Acknowledgments

The BESIII Collaboration thanks the staff of BEPCII and the IHEP computing center for their strong support. This work is supported in part by National Key R&D Program of China under Contracts Nos. 2020YFA0406300, 2020YFA0406400; National Natural Science Foundation of China (NSFC) under Contracts Nos. 11635010, 11735014, 11835012, 11922511, 11935015, 11935016, 11935018, 11961141012, 12022510, 12025502, 12035009, 12035013, 12061131003, 12192260, 12192261, 12192262, 12192263, 12192264, 12192265, 12221005, 12225509, 12235017; the Chinese Academy of Sciences (CAS) Large-Scale Scientific Facility Program; the CAS Center for Excellence in Particle Physics (CCEPP); Joint

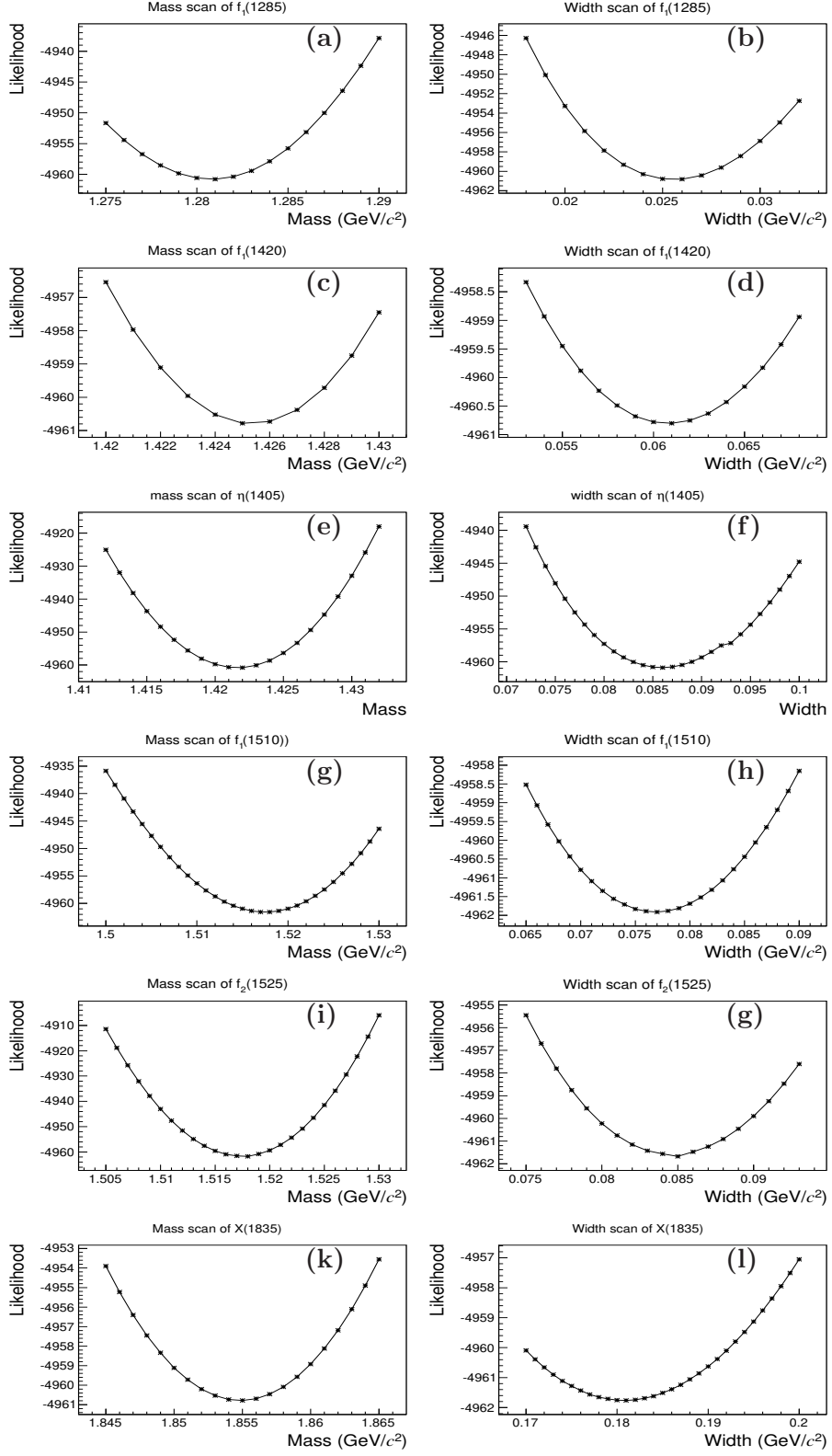
Large-Scale Scientific Facility Funds of the NSFC and CAS under Contract No. U1832207; CAS Key Research Program of Frontier Sciences under Contracts Nos. QYZDJ-SSW-SLH003, QYZDJ-SSW-SLH040; CAS Project for Young Scientists in Basic Research YSBR-101; 100 Talents Program of CAS; The Institute of Nuclear and Particle Physics (INPAC) and Shanghai Key Laboratory for Particle Physics and Cosmology; ERC under Contract No. 758462; European Union's Horizon 2020 research and innovation programme under Marie Skłodowska-Curie grant agreement under Contract No. 894790; German Research Foundation DFG under Contracts Nos. 443159800, 455635585, Collaborative Research Center CRC 1044, FOR5327, GRK 2149; Istituto Nazionale di Fisica Nucleare, Italy; Ministry of Development of Turkey under Contract No. DPT2006K-120470; National Research Foundation of Korea under Contract No. NRF-2022R1A2C1092335; National Science and Technology fund of Mongolia; National Science Research and Innovation Fund (NSRF) via the Program Management Unit for Human Resources & Institutional Development, Research and Innovation of Thailand under Contract No. B16F640076; Polish National Science Centre under Contract No. 2019/35/O/ST2/02907; The Swedish Research Council; U. S. Department of Energy under Contract No. DE-FG02-05ER41374.

References

- [1] R. L. Workman *et al.* [Particle Data Group], [PTEP **2022**, 083C01 \(2022\)](#).
- [2] M. Ablikim *et al.* [BES Collaboration], [Chin. Phys. C **44**, 040001 \(2020\)](#).
- [3] G. S. Bali *et al.* [UKQCD], [Phys. Lett. B **309**, 378 \(1993\)](#).
- [4] Y. Chen, A. Alexandru, S. J. Dong, T. Draper, I. Horvath, F. X. Lee, K. F. Liu, N. Mathur, C. Morningstar and M. Peardon, *et al.*, [Phys. Rev. D **73**, 014516 \(2006\)](#).
- [5] A. Lanaro, [Nucl. Phys. B Proc. Suppl. **136**, 56 \(1997\)](#).
- [6] K. Eberhard, Z. Alexander, [Phys. Rep. **454**, 1 \(2007\)](#).
- [7] M. Ablikim *et al.* [BES Collaboration], [Phys. Rev. Lett. **95**, 262001 \(2005\)](#).
- [8] M. Ablikim *et al.* [BESIII Collaboration], [Phys. Rev. Lett. **115**, 091803 \(2015\)](#).
- [9] B. Loiseau and S. Wycech, [Phys. Rev. C **72**, 011001 \(2005\)](#).
- [10] G. J. Ding and M. L. Yan, [Eur. Phys. J. A **28**, 351 \(2006\)](#).
- [11] J. S. Yu, Z. F. Sun, X. Liu and Q. Zhao, [Phys. Rev. D **83**, 114007 \(2011\)](#).
- [12] T. Huang and S. L. Zhu, [Phys. Rev. D **73**, 014023 \(2006\)](#).
- [13] N. Kochelev and D. P. Min, [Phys. Rev. D **72**, 097520 \(2005\)](#).
- [14] M. Ablikim *et al.* [BESIII Collaboration], [Phys. Rev. Lett. **106**, 072002 \(2011\)](#).
- [15] M. Ablikim *et al.* [BESIII Collaboration], [Phys. Rev. Lett. **129**, 042001 \(2022\)](#).
- [16] Y. Chen *et al.* [BESIII Collaboration], [Phys. Rev. D. **73**, 014516 \(2006\)](#).
- [17] V. Crede, [AIP Conf. Proc. **1182**, 471 \(2009\)](#).
- [18] M. Ablikim *et al.* [BESIII Collaboration], [Phys. Rev. D **97**, 051101 \(2018\)](#).
- [19] M. Ablikim *et al.* [BESIII Collaboration], [Chinese Phys. C **46**, 074001 \(2022\)](#).
- [20] M. Ablikim *et al.* [BESIII Collaboration], [Nucl. Instrum. Meth. A **614**, 345 \(2010\)](#).
- [21] C. H. Yu *et al.*, Proceedings of IPAC2016, Busan, Korea, 2016, doi:10.18429/JACoW-IPAC2016-TUYA01.
- [22] M. Ablikim *et al.* [BESIII Collaboration], [Chin. Phys. C **44**, 040001 \(2020\)](#).
- [23] J. Lu, Y. Xiao, X. Ji, [Radiat. Detect. Technol. Methods **4**, 337–344 \(2020\)](#).
- [24] J. W. Zhang, L. H. Wu, S. S. Sun *et al.*, [Radiat. Detect. Technol. Methods **6**, 289–293 \(2022\)](#).
- [25] X. Li *et al.*, [Radiat. Detect. Technol. Methods **1**, 13 \(2017\)](#); Y. X. Guo *et al.*, [Radiat. Detect. Technol. Methods **1**, 15 \(2017\)](#); P. Cao *et al.*, [Nucl. Instrum. Meth. A **953**, 163053 \(2020\)](#).
- [26] S. Agostinelli *et al.* [GEANT4 Collaboration], [Nucl. Instrum. Meth. A **506**, 250 \(2003\)](#).
- [27] K. X. Huang, *et al.*, [Nucl. Sci. Tech. **33**, 142 \(2022\)](#).
- [28] S. Jadach, B. F. L. Ward and Z. Was, [Phys. Rev. D **63**, 113009 \(2001\)](#); [Comput. Phys. Commun. **130**, 260 \(2000\)](#).
- [29] D. J. Lange, [Nucl. Instrum. Meth. A **462**, 152 \(2001\)](#); R. G. Ping, [Chin. Phys. C **32**, 599 \(2008\)](#).

- [30] J. C. Chen, G. S. Huang, X. R. Qi, D. H. Zhang and Y. S. Zhu, [Phys. Rev. D **62**, 034003 \(2000\)](#); R. L. Yang, R. G. Ping and H. Chen, [Chin. Phys. Lett. **31**, 061301 \(2014\)](#).
- [31] E. Richter-Was, [Phys. Lett. B **303**, 163 \(1993\)](#).
- [32] M. Williams, M. Bellis and C. A. Meyer, [JINST **4**, P10003 \(2009\)](#).
- [33] H. Albrecht *et al.*, [Phys. Lett. B **241**, 278 \(1990\)](#).
- [34] M. Ablikim *et al.* [BESIII Collaboration], [Phys. Lett. B **607**, 243 \(2005\)](#).
- [35] B. Liu, X. Xiong, G. Hou, S. Song and L. Shen, [EPJ Web Conf. **214**, 06033 \(2019\)](#).
- [36] N. Berger, B. Liu, and J. Wang, [J. Phys. Conf. Ser. **219**, 042031 \(2010\)](#).
- [37] S. Dulat and B. S. Zou, [Eur. Phys. J. A **56**, 275 \(2020\)](#).
- [38] M. Ablikim *et al.* [BESIII Collaboration], [Phys. Rev. D **93**, 112011 \(2016\)](#).
- [39] F. James and M. Roos, [Comput. Phys. Commun. **10**, 343 \(1975\)](#).
- [40] C. Robert and G. Casella, [Technometrics, **47**, 243 \(2005\)](#).
- [41] J. S. Liu, [Monte Carlo Strategies in Scientific Computing \(Springer, New York, 2001\)](#).
- [42] C. Langenbruch, [Eur. Phys. J. C **82**, 393 \(2022\)](#).
- [43] M. Ablikim *et al.* [BESIII Collaboration], [Phys. Rev. D **105**, 072002 \(2022\)](#).
- [44] S. Vanamali and G. Francesco, [Nucl. Phys. A **1037**, 122683 \(2023\)](#).
- [45] M. Ablikim *et al.* [BESIII Collaboration], [Phys. Rev. Lett. **115**, 091803 \(2015\)](#).
- [46] M. Ablikim *et al.* [BESIII Collaboration], [Phys. Rev. D **95**, 032002 \(2017\)](#).
- [47] M. Ablikim *et al.* [BESIII Collaboration], [Chinese Phys. C **46** 074001 \(2022\)](#).
- [48] M. Ablikim *et al.* [BESIII Collaboration], [Phys. Rev. D **83**, 112005 \(2011\)](#).
- [49] M. Ablikim *et al.* [BESIII Collaboration], [Phys. Rev. D **81**, 052005 \(2010\)](#).
- [50] M. Ablikim *et al.* [BESIII Collaboration], [Phys. Rev. D **87**, 012002 \(2013\)](#).
- [51] Hechenberger, Florian and Leutgeb, Josef and Rebhan, Anton, [Phys. Rev. D **107**, 114020 \(2023\)](#).

A Scan Plots For Baseline Solution



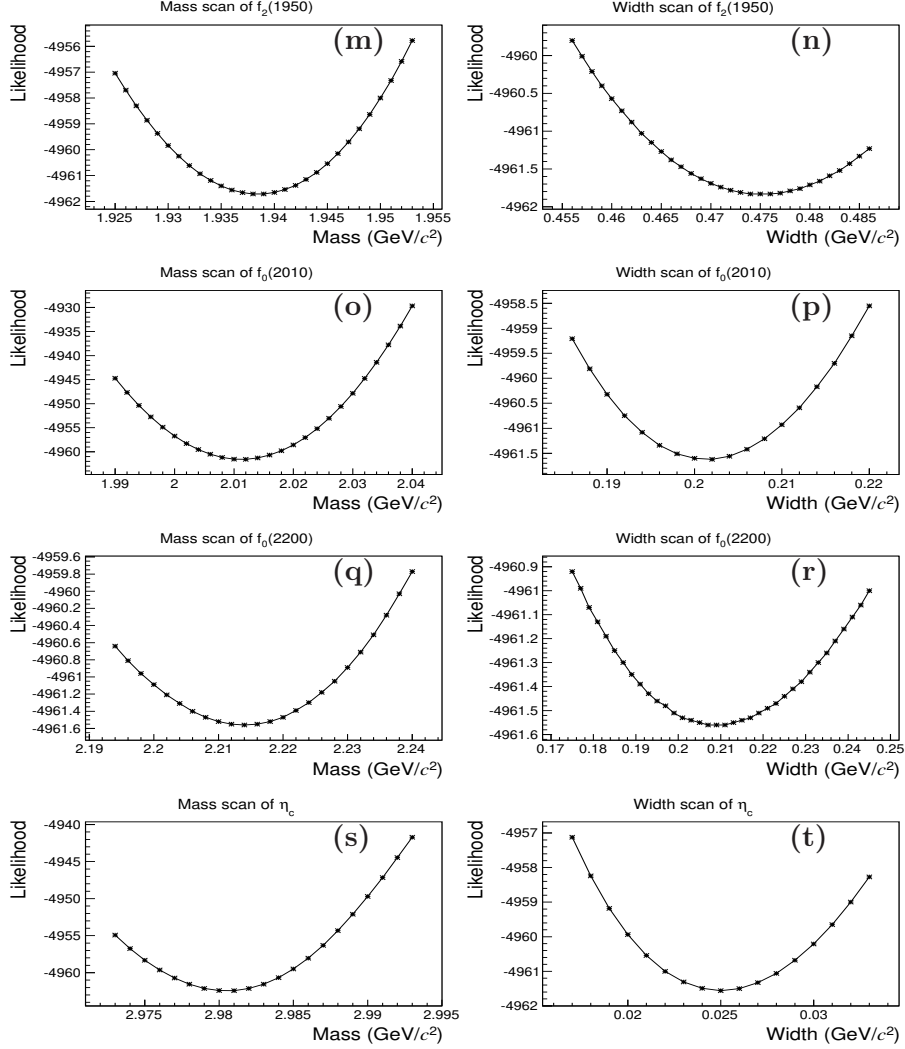


Figure 5: The optimization plot for each resonance. (a)(b) Mass/Width scan of $f_1(1285)$. (c)(d) Mass/Width scan of $f_1(1420)$. (e)(f) Mass/Width scan of $\eta(1405)$. (g)(h) Mass/Width scan of $f_1(1510)$. (i)(g) Mass/Width scan of $f_2(1525)$. (k)(l) Mass/Width scan of $X(1835)$. (m)(n) Mass/Width scan of $f_2(1950)$. (o)(p) Mass/Width scan of $f_2(2010)$. (q)(r) Mass/Width scan of $f_0(2200)$. (s)(t) Mass/Width scan of η_c .